Reaction of the Marcellus Shale with hydraulic fracturing fluid, an experimental study

Brittany Jane McManus

A report prepared in partial fulfillment of
the requirements for the degree of

Master of Science
Earth and Space Sciences: Applied Geosciences

University of Washington

December 2017

Project mentor:
Johnathan Moore

Reading committee:
Juliet Crider
Katharine Huntington

MESSAGe Technical Report Number: 059

Abstract

Technological advancements in the oil and gas industry in the past few decades have led the Marcellus Shale to be one of the most productive unconventional reservoirs in the United States. Increased production has resulted in more fundamental questions regarding how the fluids being injected interact with the reservoir. Previous research at the National Energy Technology Laboratory experimentally characterized the geochemical and physical changes to the Marcellus Shale as a function of rock reaction with hydrofracturing fluids of various compositions, based on average compositions used in the Appalachian Basin. In these studies, synthetic fracking additives were mixed up to 3 weeks prior to experimental operations and then injected into Marcellus Shale cores. This is in contrast to field operations where mixing of chemicals typically happens at the wellhead as fracking operations commence. Observed variations in dissolution and precipitation in these experiments is potentially due to time differences between mixing and injection; it is possible that the additives are degrading over time. In the current study, synthetic fracturing fluids of the same composition, as the previous studies (excluding ammonium persulfate) were prepared and then immediately injected into artificually fractured Marcellus Shale cores. Marcellus Shale cores were held at representative conditions of 150°F, pore pressures of 2800 psi, and confining pressures of 3000 psi. Mineral dissolution and precipitation inferred from computed tomography (CT) images in conjunction with mineral saturation indices calculated from ion chromatography (IC), inductively coupled plasma mass spectrometry (ICP-MS), and inductively coupled plasma optical emission spectroscopy (ICP-OES) of the reacted fluids were used to characterize the chemical and physical changes in the rock as a function of time exposed to fracturing fluid. The reactivity of the fracturing fluid with ammonium persulfate with the Marcellus Shale can be related to changes in time between preparing the fracturing fluid and injection. Without the ammonium persulfate additive, temporal variations in preparing and using the fluid did not influence barite precipitation. Instead the composition of the Marcellus Shale proved to be the dominant control on mineral dissolution. Ammonium persulfate appears to drive important chemical and physical changes though. Given hydraulic fracturing fluid prepared within an hour of use without ammonium persulfate, the guar gel additive, used to increase viscosity for proppant placement, did not degrade, potentially preventing chemical reactions and removing proppant. Results from this study provided insight on fluid stability relative to temporal changes in preparing synthetic fracturing fluid in laboratory studies on fluid-rock interactions.

Table of Contents

Pages

List of Figures

Pages

List of Tables

Acknowledgements

Thanks to the Mickey Leland Energy Fellowship, I had the opportunity to work on a project with the Department of Energy at the National Energy Technology Laboratory in Morgantown, WV.

An immense thank you goes to my mentors Johnathan Moore and Juliet Crider for answering all of my questions and supporting me on this project.

Thanks to my friends and family for putting up with my anxiety over school.
I promise this is my last degree!

Introduction

Over the past few decades, the oil and gas industry has rapidly increased production, due to technological improvements in hydraulic fracturing methods. Advancements in natural gas recovery from unconventional reservoirs has made the Marcellus Shale an economically important resource. Production of the Marcellus Shale has also increased research into subsurface fluid interaction with the reservoir. Recently, workers have begun to catalogue dissolution and precipitation changes to the reservoir with variations in the hydraulic fracturing fluid in laboratory experiments (Vankeuren et al., 2017; Hakala et al., 2017; and Moore et al., 2017). Variations in fracturing fluid can be related to changes in mineral saturation indices derived from a combination of computed tomography (CT) and geochemical analyses. Mineral saturation, which drives precipitation and accounts for mineral dissolution, can provide insight into permeability changes.

Previous experiments studied variations in hydraulic fracturing fluid composition with slight variations in experimental, methods but a comparison of temporal variations between experiments was not completed. Vankeuren et al. (2017) used fracturing fluid prepared a day before running fluid flow tests. Their results showed dissolution of calcite but also precipitation of barite, which reduced permeability. Moore et al. (2017) used fracturing fluid prepared up to three weeks before running the fluid flow test and found very little barite precipitation but still had calcite dissolution. Both tests used the same fracturing fluid and Marcellus Shale samples from the same site. Hakala et al. (2017) ran fluid flow tests with hydraulic fracturing fluid used to develop the Marcellus Shale Energy and Environmental Laboratory (MSEEL) MIP 3H well in 2015.

To identify if there are temporal limitations to the effectiveness of fracturing fluid to have a desirable reaction with the reservoir, I completed two additional tests, test 5 and test 6, using fracturing fluid that was prepared within an hour of use. Results contribute toward understanding the temporal stability of fracturing fluid, which can provide insight for future tests on variable components in a complex system.

Background

Geologic History and Composition of the Marcellus Shale

The Marcellus Shale is found in the Appalachian Basin, which formed around 440-480 million years ago, when the passive Appalachian plate margin became an active subduction zone as the Rheic Ocean began to close (Clark, accessed August 2017; Harper and Kostelnik, accessed September 2017; USGS, accessed October 2017). Small continents and islands were added onto the Appalachian margin while the Acadian Mountains formed (Harper and Kostelnik, accessed September 2017). A foreland basin formed, creating the Appalachian Basin, covered by several shallow inland seas (Harper and Kostelnik, accessed September 2017; Figure 1). As the Acadian Mountains were weathered, rivers deposited sediment along the eastern edge of the basin, forming the Catskill delta (Milici and Swezey, 2006; Harper and Kostelnik, accessed September 2017). The Marcellus Shale is at the base of the Catskill delta and was probably deposited in the deep water of the forming foreland basin (Milici and Swezey, 2006). The basin began to subside

on the eastern edge due to increased deposition. Continued burial of the basin allowed thermal maturation of the organic rich shale, leading to the energy resource that is extracted today.

The Marcellus Shale formation underlies five US states: New York, Pennsylvania, Ohio, West Virginia, and Kentucky. The formation is divided into two sections, lower and upper. The lower section has a higher organic content than the Upper Marcellus Shale (Energy Information Administration, 2017). Due to the geologic history of the area, the Marcellus Shale is thickest near the present-day Appalachian Mountains (Figure 2). Given the subsidence of the basin in the east, the formation is buried deepest along the Appalachian Mountains and becomes shallower to the west. Outcrops of Marcellus Shale can also be found in the folded remnants of the Appalachian Mountains due to continued orogenic events following the deposition of the Marcellus Shale.

The mineral composition of the Marcellus Shale can vary widely over a short distance. Wang et al. (2012) compared data from 195 Marcellus Shale core samples and found a variety of minerals including quartz, calcite, dolomite, illite, chlorite, and others. Additionally, the volume percent of the minerals identified could vary with some ranging from one percent to eighty (Wang et al., 2012). Vankeuren et al. (2017) used Marcellus Shale samples from New Bedford, PA and measured mineral content of 50% clay (35% illite, 7.5% ilite-smectite, and 7.5% chlorite), 25% calcite, 20% quartz, and 5% pyrite.

Hydraulic Fracturing Industry in Appalachia

New drilling methods in hydraulic fracturing (fracking) have made the Marcellus Shale formation a highly productive source of natural gas in the United States (Energy Information Administration, Natural Gas Explained; Figure 3). Demand for natural gas is expected to increase to 385 billion m^3/yr by 2035 as coal power plants are converted to natural gas, new pipelines come online, and liquefied natural gas export facilities open up (Stringfellow, et al., 2014; Hodge, 2016). Development of natural gas wells in Marcellus Shale will continue due to economic demand. Although production of natural gas has increased rapidly over the last few decades, little is known about how variations in fracturing fluid can alter fluid-rock interactions within the reservoir.

Fracking has become an economically successful method to stimulate production of natural gas and petroleum from unconventional reservoirs. Fracking involves drilling horizontal wells in reservoirs with low permeability and creating artificial fractures using fluids. The fractures created are propped open using proppant, typically quartz sand. Natural gas production in the Marcellus Shale requires the use of thousands of gallons of water to be mixed with fracturing fluid additives and proppant. Hydraulic fracturing fluid varies at each well, depending on the reservoir and the additives used by the drilling company. Common additives used in industry have been identified by Fracfocus.org and by academic studies on hydraulic fracturing fluid (Al-Muntasheri, 2014; Donaldson, et al., 2013). The mixed fluid is injected into the reservoir to decrease friction between fluids and solid surfaces, prevent scaling (mineral precipitation that would occlude porosity), reduce microbial growth (which could limit the effectiveness of additives and reduce productivity), and to increase permeability of the reservoir. Around 4.5 million gallons of fluid is used per well in Pennsylvania with 10-80% of the fluid

returning to the surface (Ferrar, et al., 2013). Water that returns to the surface, known as "produced water," is made up of formation water and flowback (Vankeuren et al., 2017). The formation water comes from the formation being produced and tends to have a high salinity (Orem et al., 2014). Flowback is the fluid pumped into the formation during fracking which returns to the well head (Orem et al., 2014). A common step in fracking involves a shut-in period which can last from a few days to several months (Fakcharoenphol et al., 2016). During the shut-in period, fluids have more time to react with the shale, potentially increasing permeability and natural gas production (Fakcharoenphol et al., 2016). Additionally, the shut-in period allows time for further well production setup (Liu et al., 2015).

Disposing of the large volume of waste fluid used in fracturing the Marcellus Shale has proven difficult. In 2011, the Pennsylvania Department of Environmental Protection halted further disposal of wastewater from the Marcellus Shale at wastewater treatment plants (Ferrar, 2013). A chemical analysis of treatment plant effluents found components of fracking fluid, including barium, strontium, bromides, chlorides, total dissolved solids, and benzene, at levels above water quality criteria set by the Environmental Protection Agency (Ferrar, 2013). With limited access to water treatment facilities, the 570% increase of wastewater production in the Pennsylvania region means surface and subsurface wastewater storage has become more common (Lutz, et al., 2013). The high levels of total-dissolved-solids (TDS) and barium found in stored wastewater have caused concerns about aquifer contamination risks. Renock (2015) determined that the barium found in the wastewater is from reactions of hydraulic fracturing fluid with the reservoir rocks and not from surface water mixing with the reservoir brine.

By understanding subsurface interactions between hydraulic fracturing fluid and the reservoir rock, reservoir management could be improved. Improving reservoir management could increase production from each well in the Marcellus Shale play thus reducing the amount of wastewater containing high levels of total-dissolved solids (Ferrar et al., 2013; Vankeuren et al., 2017). Production could be improved by preventing precipitation of scaling in the hydraulic fractures by decreasing bulk export of dissolved solids from the reservoir. Additionally, understanding how to mediate these reactions would potentially allow producers to reuse wastewater for multiple hydraulic fracturing operations, further reducing the total amount of water used.

To better understand fracking in Appalachia, experimental studies of fracking fluid-Marcellus Shale reactions have been conducted on core samples through the Marcellus Shale Energy and Environmental Laboratory (MSEEL). MSEEL is a long-term field study of a hydraulically fractured natural gas well involving West Virginia University, Northeast Natural Energy, NETL, and Ohio State University (Stair et al., 2017). A wide range of variables in well development and production have been recorded and studied by MSEEL, including the hydraulic fracturing fluid, reservoir host rock (Marcellus Shale), and air quality. The MSEEL MIP 3H well was drilled in the Marcellus Shale reservoir in November of 2015 (Hakala et al., 2017). The MIP 3H well core was preserved and slabbed for future studies, including fluid flow tests and CT scanning. Hydraulic fracturing fluid from well production was collected and used in a follow-up study by Hakala et al. (2017).

From the MSEEL project, a complete list of chemicals used for well production was

recorded and samples were collected for future tests (Table 1). The purpose for the additives used for the MSEEL well was listed as: corrosion inhibitor, scale inhibitor, biocide, antifoam agent, acid, breaker, gelling agent, friction reducer, iron control agent, and fluid loss additive (Table 1). Corrosion inhibitors, typically a proprietary blend, are added to prevent corrosion of drilling equipment and well casings from acids, salts, and other corrosive additives (Stringfellow et al., 2014). Propargyl alcohol and thiourea, two common corrosion inhibitor components, were used in the MSEEL fracturing fluid (Stringfellow et al., 2014). Scale inhibitors, like ethylene glycol used in the MSEEL fluid, prevent the precipitation of minerals in the fluid that could cause a decrease in porosity and thus a decrease in gas production. The common biocide, Glutaraldehyde, is used to prevent bacteria from growing which could degrade the chemical additives (Stringfellow et al., 2014). Acids are added to hydraulic fracturing fluids to adjust pH, to clean the wellbore, and to dissolve minerals in the reservoir (Stringfellow et al., 2014). Adjusting the pH prevents other additives in the fluid from breaking down (Stringfellow et al., 2014). Increasing the viscosity by using a gelling agent or guar gum prevents proppant from dropping out of the fluid. Once the proppant is in position, propping open fractures, a breaker is then used to reduce the viscosity of the fluid. Oxidizers, such as persulfates, break down guar based polymers which reduces the viscosity (Al-Muntasheri, 2014). Friction reducers are added in to reduce fluid surface tension (Stringfellow et al., 2014). Iron control additives prevent iron from precipitating out and reducing permeability (Stringfellow et al., 2014).

Chemical components added during fracking are listed on FracFocus.org for individual hydraulically fractured wells in the United States. Although FracFocus.org provides an enormous amount of data, not all states require reporting to the website and the total chemical composition of hydraulic fracturing fluids is not fully described because of the use of proprietary additives.

Given the available information, researchers at the Department of Energy have conducted several experiments to document how variations in hydraulic fracturing fluid alters the reaction between the fluid and the Marcellus Shale at reservoir conditions. Experiments conducted by Vankeuren et al. (2017), Moore et al. (2017), and Hakala et al. (2017) all used Marcellus Shale cores that were synthetically fractured using the Brazilian method, applying enough pressure along the length of the cores using a stone splitter to split the cores close to the middle (Atkinson et al., 1982). Quartz sand proppant was packed into the fracture for each core, propping open the fractures. All three experiments used mixed hydraulic fracturing fluid rather than reacting individual additives with the Marcellus Shale. A fluid flow system was used in each setup, with the hydraulic fracturing fluid pumped through the cores and into a set of back pressure pumps (Figure 4). The fluid was kept in an airtight container with the headspace filled with nitrogen gas. The experiments aimed to represent field conditions including conditions at depth where the fluid would be interacting with the reservoir rock. The rock cores were put under pressure and heat to simulate reservoir conditions. Because these studies are important foundations for my work, I review them in turn.

(1) Vankeuren et al. 2017: Day-old hydraulic fracturing fluid

A fluid-rock interaction study completed by Vankeuren et al. (2017) tested four fluids: local spring water with hydraulic fracturing fluid chemicals, synthetic reused produced water, synthetic reused produced water with hydraulic fracturing fluid chemicals added, and synthetic

reused produced water with hydraulic fracturing fluid chemicals added without hydrochloric acid (2017). The synthetic reused produced water was based on hydraulic fracturing fluid samples from wells in Pennsylvania and were created using salts and natural spring water (Vankeuren et al., 2017). Hydraulic fracturing fluids were mixed a day before starting the tests. A control test with just local spring water was also completed. Marcellus shale cores were used in a shut-in period of one week with a simulated reservoir with a temperature of 66^{o} C and pressure of 20 MPa (Vankeurean et al., 2017).

Reservoir reactions were documented using an industrial CT scanner and geochemical analysis of the fluid. Results from the tests found calcite dissolution occurred with the presence of hydrochloric acid in the hydraulic fracturing fluid and increased the fracture volume (Figure 5). When produced water was reused with hydraulic fracturing fluids added in there was an increase in mineral precipitated, notably barite.

(2) Moore et al. 2017: Three-week old hydraulic fracturing fluid

Moore et al. (2017) completed four additional experiments using deionized (DI) water instead of local spring water. The hydraulic fracturing fluid additives used were the same as in Vankeuren et al. (2017), but the fluid was mixed up to three weeks before starting the tests. Marcellus Shale cores were used and reservoir conditions were simulated with a temperature of 65^{o}C (150^{o}F), a confining pressure of 20 MPa (3,000 psi), and a pore pressure of 19 MPa (2,800 psi) (Moore et al., 2017). Cores were scanned before and after the tests using an industrial CT scanner. Images were then processed using ImageJ and Ilastik. In contrast to the results from Vankeuren et al. (2016), there was less barite precipitation but calcite dissolution did still occur.

(3) Hakala et al. 2017: Years old hydraulic fracturing fluid

Three simulated four-day shut-in tests were carried out using 2015 hydraulic fracturing fluid from the MSEEL MIP 3H well (Hakala et al., 2017, Table 1). Reservoir conditions were simulated with a core temperature of 150^{o}F, a confining pressure of 3000 psi, and a pore pressure of 2800 psi (Hakala et al., 2017). Two tests used rock core samples from the MIP 3H rock core slab while the third test was run without a rock core (Hakala et al., 2017). The rock cores were taken from 7498.4 ft. and 7504.6 ft. which was near where hydraulic fracturing occurred for the MIP 3H well (Hakala et al., 2017).

Geochemical analysis of the fluid samples included ion chromatography (IC), inductively coupled plasma mass spectrometry (ICP-MS), and inductively coupled plasma optical emission spectroscopy (ICP-OES). Additionally, before and after images were taken using an industrial CT scanner. The results from this experiment showed an increase in calcium in the fluid after contact with the shale, suggesting dissolution of calcium carbonate, most likely calcite (Hakala et al., 2017). Unlike the earlier two experiments (Vankeuren et al., 2017; Moore et al., 2017), there was no observable precipitation of secondary minerals, including barite (Hakala et al., 2017). Due to the difference in the fracturing fluid used and the time between preparation and use, the observed variation in secondary mineral precipitation could not be attributed to one variable.

Methods and Assumptions

Overview

In collaboration with the Geomaterials Characterization, Analytics and Modeling group at NETL, I completed two fluid-rock interaction tests in June and July of 2017, using synthetic fracturing fluid and Marcellus Shale cores. To compare hydraulic fracturing fluid variations, I used the same fluid flow system and sampling methods as previous experiments. Working with Johnathan Moore, who directed tests 1-4, the two pairs of cores I used were labeled core sets 5 and 6, continuing the series of tests conducted at NETL in Morgantown, WV. For each test there were two cores, labeled 5.1 and 5.2 for test 5 and 6.1 and 6.2 for test 6.

As in previous experiments, the Marcellus Shale cores were scanned using an industrial CT scanner to capture before and after images of the fracture. The images were used to identify and characterize the volume of chemical alterations to the matrix, to identify compositional variations between cores, and to document secondary fractures, potential flow paths, and the fracture surface.

Fluid samples were collected based on a sampling schedule used in earlier experiments. Fluids were taken from the reservoir (location A), from the back pressure pumps (location B), and from the confining pressure pumps (location D) (Figure 4). Samples were sent to the National Energy Technology Laboratory in Pittsburgh, PA for geochemical analysis (IC, ICP-MS, and ICP-OES), to confirm chemical reactions observed in the CT scans and to characterize additional reactions not observed in the images.

Initial System Setup

With the help of Johnathan Moore, the fluid flow system was assembled and cleaned to prevent cross contamination from previous tests. Residual air in the tubes feeding the fluid through the system was removed and the pumps and tubes were cleaned by flowing Alconox detergent mixed in DI water through the system before being flushed with just DI water. The end bells and the Buna-N rubber casings used to hold the rock cores were also washed with Alconox and DI water (Figures 6-7). The confining pumps were then filled with DI water.

Rock Core Prep

For tests 5 and 6, four rock cores were used, each around 2 inches long with a diameter of 1.5 inches. Rough ends of the rock core were cut using a rock saw or were polished. The rock core ends were smoothed down and flattened to allow the end bells and cores to be flush against each other. The rock cores were cleaned using DI water and allowed to dry overnight.

The surface of the fresh fracture on one half of the cores was wetted with DI water before applying a one-to-two grain layer of proppant, in this case UniFrac 40/70 mesh northern white sand that is >99% quartz (Vankeuren et al., 2017, p. S6; Figure 8). The other halves without proppant were placed on top of their corresponding halves and held flush. Any proppant outside of the fracture was removed using paper towels. The first rock core was gently pushed into the

rubber casing, with the fracture horizontal (Figure 9). A ruler was used to push the core flush against the end bell. A second core, with the fracture horizontal and aligned with the horizontal fracture of the first core, was gently pushed into the same casing until flush against the first rock core piece. While pushing the cores into position, I felt for any grinding which could indicate sand grains were on the outside of the rock cores. Sand grains located outside of the fracture can prevent a water-tight seal and allow fluid to flow outside of the fracture. The second end bell was pushed into the rubber casing until flush against the rock core. More tape was wrapped on the outside to prevent the core from moving and the end bells from slipping out during transportation to and from the industrial CT scanner. The second rubber casing was similarly prepared, creating two 4-inch-long cores labeled 5.1 and 5.2, for Test 5, and 6.1 and 6.2, for Test 6.

Fluid Flow Tests

On the first day of the five-day shut-in test, I mixed together the synthetic fracturing fluid. Chemicals were shipped from the NETL lab in Pittsburgh, PA with the solid chemicals mixed together and the liquid chemicals separate (Table 3). The same synthetic fracturing fluid composition was used in previous fluid flow tests at NETL and was based on the MSEEL project fracturing fluid for well MIP 3H and commonly used additives listed on FracFocus.org (Table 1). Once mixed together the fluid was placed on a hot plate with a magnetic stirrer to prevent the fluid from separating. The top of the glass beaker holding the synthetic fracturing fluid was sealed and nitrogen gas pumped in slowly to fill in the head space (Figure 10). Nitrogen gas was used to prevent further oxygen dissolving into the fluid and to simulate an anoxic environment of a natural gas reservoir (Vankeuren et al., 2017). The tubes leading to the pumps were then removed from the brine fluid and attached to the seal on the beaker to begin pumping synthetic fracturing fluid through the system. Residual air from disconnecting the tubes needed to be removed before setting the pumping rate for both pumps to 0.03 mL/min.

Each day of the test, fluid samples were taken from the back pressure pumps, labeled as sampling location B with Core 1 labeled as B1 and Core 2 labeled as B2 (Figure 4). Fluid samples were taken from the reservoir, labeled as sampling location A, on everyday (Figure 4). Fluid samples from the confining pumps, labeled as sampling location D with Core 1 labeled as D1 and Core 2 labeled as D2, was collected on the first and last days of the tests. Smaller sample volumes had to be collected on days 1, 2, and 4 to prevent emptying the back pressure pumps.

Fluid samples were collected for IC, ICP, isotopes of carbon, oxygen and strontium, pH, and temperature tests. Fluid samples for IC, ICP, Sr Isotope, and pH and temperature were collected using 100 mL plastic syringes for large sample days and 10 mL plastic syringes on small sample days. IC, ICP, and Sr Isotope samples were weighed and recorded (Tables 3-5 and 7-9). The smaller samples were diluted with DI water and the Sr Isotope and ICP bottles were acidified with nitric acid. Nitric acid, which is free of metals and other contaminates, was used to break down the metals in the fluid. Temperature and pH were recorded using around 1 mL of the fluid sampled from all three locations (Tables 6 and 10). Oxygen isotope and carbon isotope samples were collected using a 1 mL glass syringe and injected into acid washed glass test tubes using a needle. 0.5 mL was used for the oxygen isotope fluid samples and 0.75 mL was used for the carbon isotope fluid samples. IC, ICP, and strontium isotope samples were shipped to the NETL Pittsburgh, PA lab for analysis. The oxygen and carbon isotope fluid samples were sent to

the geochemical labs at West Virginia University for a study on water contamination from natural gas wells.

Test 5

The four Marcellus Shale cores used in test 5 were selected from pre-cored samples taken from an outcrop in Pennsylvania. Cores from Pennsylvania were used due to their availability, providing a trial run while I learned how to conduct the experiment. Additionally, the cores provided an opportunity to compare how compositional variation in the Marcellus Shale formation can alter fluid-rock interactions. The cores lacked natural fractures and had to be artificially fractured using the Brazilian method (Vankeuren et al., 2017; Atkinson, Smelser, and Sanchez, 1982; Figure 11). Blue painting tape was temporarily used to hold the core pieces together after being fractured.

To compare how the Marcellus Shale physically changed when exposed to hydraulic fracturing fluids, CT images were taken of the cores before and after the experiments. Pre-test images of the cores were taken using a North Star Imaging, Inc. industrial x-ray CT scanner with an optimal voxel size of 23.3 microns. The two cores, 5.1 and 5.2, were scanned in two sections, with the bottom half of each core designated as the inlet and the top half of each core as the outlet. CT images were then calibrated by Johnathan Moore before I uploaded them into ImageJ, a free image processing program (Appendix A). Image processing was completed using ImageJ and Ilastik (Appendix A).

For test 5, the fluid flow system was slowly brought up to experimental pressure and temperature levels, allowing time for me to familiarize myself with the system and to check the equipment for leaks and errors. To prepare for running test 5, DI water was initially used to flow through the cores while the cores were slowly put under pressure over the span of two days, allowing time for any leaks to be fixed. Both cores had small leaks: core 1 had a leak of 8×10^{-4} mL/m and core 2 had a leak of 9×10^{-4} mL/m. Neither leak was great enough to prevent collecting enough fluid for analysis during the test. Once the cores were under 3000 psi and there were no new leaks, the DI water was switched out for brine and the cores were brought up to 150^{o}F. The brine was then replaced with synthetic fracturing fluid which flowed through the cores for four days, for a total of around 96 hours.

With the completion of the fluid flow test, the confining pressure on the rock cores was reduced and the heat turned off. Alconox mixed with DI water was again used to clean the fluid flow system before being flushed with DI water. The confining pumps were not drained.

The rock cores were scanned again using the industrial CT scanner to produce post-experiment images. The optimal voxel size was 23.3 microns. The same image processing was applied to the post-experiment images as the pre-experiment images, with the additional segmentation of the reaction rim (Appendix A). Additional quantitative analysis was also completed on the reaction rim along the fracture surface of the cores.

Test 6

For test 6, Marcellus shale rock cores were cut from the MSEEL MIP 3H well core. From the MSEEL MIP 3H well core, two rock core samples were taken from around 7,493.4 ft. and two other cores were taken from 7,497.9 ft. The location was selected near earlier test sampling locations around 7,498.4 ft. and 7,504.6 ft. (Hakala et al., 2017). Cores were drilled parallel to bedding with natural horizontal fractures in the middle of the cores. Each core piece was around 2.75 inches long with a diameter of 1.5 inches. MSEEL MIP 3H paperwork was also completed and submitted for the samples taken.

Due to the natural fractures in the cores, rock cores 6.1 and 6.2 did not need to be artificially fractured. The rock cores were scanned using the industrial CT scanner with an optimal voxel size of 32.9 microns

The fluid flow test used the same chemical components as test 5 and were mixed together on the first day of test 6. Fluid samples for IC, ICP, Strontium, oxygen, and carbon isotopes, pH, and temperature were all collected and recorded using the same methods as test 5 (Tables 8-11).

On day three of test 6, the pump for core 6.1 failed due to an increase in pressure. Several hours were spent attempting to trouble shoot the problem. At first it was assumed there was an air bubble in the line. After suctioning out any air the pump, the pump continued to fail. Next it was hypothesized there was a clog in the line. To try and clear the clog the flow rate was increased and the metal lines were repeatedly struck but the pump still failed. Disconnecting the lines before and after the core it became apparent there was flow getting to the core but no fluid was exiting the core. Core 6.1 was removed from the system and examined for clogs along the endbells. When the rock core was opened up, I observed that there was no longer any proppant in the fracture. I inferred that this allowed the fracture to close under pressure, preventing fluid from moving across the sample. To resolve this problem, more proppant was added to the fracture and the test for core 6.1 was restarted and allowed to run over the weekend for a total of around 170 hours. Core 6.2 ran for around 96 hours.

Post-experiment scans were taken of the rock cores, and image processing was completed to calculate the amount of proppant, identify where proppant remained, and to calculate the volume of the core that reacted. The fluid flow system was cleaned again with Alconox mixed with DI water before being flushed with DI water. Fluid samples were sent to their corresponding labs for geochemical analysis.

Results

Observations of the Rock Cores Before and After Flow Test

Prior to the experiments, the Marcellus Shale rock cores used in tests 5 and 6 were dry and black in color. The cores were drilled parallel to bedding but the bedding was not easily distinguishable when looking at the core samples. There were some concentrated layers of calcium carbonate minerals up to 3mm in size with most crystals < 1mm. The MSEEL sample, used in test 6, had some framboidal pyrite visible on the fresh fracture surface (Figure 12). On

the CT images, there were calcium carbonate veins and concentrated areas of calcium carbonate minerals (Figure 13). The fracture surface on the manually fractured cores was rough and slightly stepped. For the MSEEL samples, the fracture was slightly smoother. The fracture surface in the CT scans varied along the length of the cores, with smooth, straight sections, as well as stepped and curved sections.

After the tests, there was no mineral precipitation observed on the endbells or on the rock cores. Additionally, there did not appear to be any oxidation of the pyrite along the fracture surface of the rock cores. In test 6 some of the proppant became imbedded in the Marcellus Shale along the fracture surface. In the test 5 CT images there was a visible reaction rim along the fracture and along a secondary fracture in the bottom halves of the cores. In the test 6 CT images there was very little visible reaction along the fracture.

Observations of the Experimental Fluid

While pulling fluid samples, Johnathan Moore observed the fluid from the sample location A was more viscous than previous tests. When pulling fluid samples from sample location B, black grains were visible in the glass syringe fluid.

pH Results for Tests 5 and 6 relative to time

To compare how pH changed, I graphed my pH measurements for the reservoir (sampling location A) and the back pressure pumps (sampling locations B1 and B2) for tests 5 and 6. Samples from the reservoir remained stable and acidic throughout both tests (Figure 14). At sampling location B, fluid from test 5 was more neutral with a slight decrease in pH over the span of the test. Test 6 was extended due to a pump failure. At sampling location B for test 6, the pH varied between the two cores. Fluid from core 6.2 remained stable but acidic while fluid from core 6.1 was more neutral but became more acidic over time.

pH data from tests 3 and 4 conducted at NETL were available to me. I compared pH between test 3, 4, and 5 from fluid taken at the reservoir and the back pressure pumps (Figure 15). For all three experiments, the reservoir fluid (location A), remained acidic. Fluid from the back pressure pumps (locations B1 and B2) for all three tests were all more neutral and closely grouped together. In each test, the fluid sampled from B2 was slightly more neutral than B1.

CT Results and Volume Estimates for Proppant and Reaction Rim

From the CT images, I characterized the volume of proppant and reaction rim to quantify changes to the fracture in cores 5.1 and 5.2 after the experiment. Due to the lack of reaction in the top halves of the cores in reaction 5, the volume of reaction rim and proppant were not measured for the top halves. All segments from test 6 had a lack of visible reaction and could not be measured. Measurements of the proppant area and the reaction rim for each image slice were exported from ImageJ into an Excel sheet. Multiplying the proppant area and the reaction rim area by the resolution cubed gave the volume of proppant and reaction rim throughout the rock cores. The proppant volume and the reaction rim volume were then graphed together (Figure 16).

The volume of rock reacted was highest in test 5 where the fluid first comes into contact with the cores, the inlet end of the core. For core 5.1, the volume of reacted rock decreased rapidly away from the inlet and remained below 0.1 mm^3 with a low around 0.04 mm^3 (Figure 16a). The proppant volume for core 5.1 remained small except at two locations where the volume increased briefly. Where the proppant volume increased, the reaction volume also increased. Unlike core 5.1, the reaction volume in core 5.2 remained mostly above 0.1 mm^3 for the first 15 mm (Figure 16b). The reaction volume had a low around 0.01 mm^3 near the end of the outlet of the core. At 31 mm from the inlet, there is a spike in the reaction volume. The volume of proppant was highest near the inlet and gradually decreased until reaching a low but steady volume after 15 mm.

I used the reaction rim data from tests 3 and 4 to create comparisons between tests. Reaction rim fractional area in transverse cross section was calculated for each core for tests 3, 4, and 5. Test 6 was not calculated due to the lack of reaction. The fractional area was calculated by exporting the area of the image, the % area of the fracture outline, and the % area of the fracture outline that reacted. The area was then calculated for the fracture outline and the fracture outline reacted. The area reacted was then divided by the fracture outline area. Each test's cores were then graphed (Figures 17-18) to show variation along the length of the core from the inlet to the outlet. The amount of reaction between the calcium carbonate minerals and the hydraulic fracturing fluid depended on the distance from the inlet. In test 5, the amount of reaction was substantially higher near the inlet and then tapered off through the length of the core (Figure 18). The top halves of both cores, closer to the outlet, in test 5 did not have a reaction rim. Test 4 and 5 had the most amount of reaction near the inlet while the amount of reaction along the fracture surface increased further away from the inlet in test 3. The reaction along the fracture surface in test 5 had a wider range and was more variable than tests 3 and 4 (Figure 18).

The reaction area along the rim varied not just between tests but also between cores in each experiment. The cores in Test 3 and 4 were drilled differently with respect to bedding, with one core drilled parallel to bedding and the other drilled perpendicular to bedding. In Test 3 the core drilled parallel to bedding had some fluctuation in reaction which was relatively small when compared to the high variability in reaction for the core drilled perpendicular to bedding (Figure 17a). Test 4 also had one core drilled parallel to bedding and one drilled perpendicular to bedding. Both cores had some fluctuation in reaction but neither core had as much variation as seen in Test 3. The difference in reaction between the two cores in Test 4 though is around 20%, with the core drilled perpendicular to bedding more reactive throughout the experiment than the core drilled parallel to bedding (Figure 17b).

Geochemical Results and Mineral Saturation Index Calculations

Results from ICP-OES, ICP-MS, and IC provided chemical species concentrations in the fluid samples. Here I report results for calcium, iron, sulfate, and barium. Graphs of the concentration versus time were made for each chemical species for tests 5 and 6 (Figures 19-20). Sulfate was below detection levels in test 6 and no graph was created. The four chemical species concentrations were used to identify calcium carbonate dissolution, barite precipitation, and pyrite oxidation. In test 5, calcium in the reservoir (location A) remained stable at around 2.5 x 10^6 ug/l, well below the calcium concentration from fluid samples taken from the back pressure

pumps (location B; Figure 4) for cores 5.1 and 5.2. Overall, calcium concentration in the fluid from the back pressure pumps for cores 5.1, 5.2, 6.1, and 6.2 increased over time. The calcium concentration for the reservoir during test 6 did not remain stable but instead decreased on two of the five days. Sulfate concentration slightly decreased in the reservoir during test 5 but during test 6 the concentration of sulfate was below detection levels and was not graphed. Sulfate concentrations measured from the back pressure pumps was variable throughout test 5 and between the two cores. Fluid from core 5.1 peaked in sulfate concentration on day two and then slowly decreased while fluid from core 5.2 at first decreased before increasing to a high of over 1.0×10^5 ug/l but did eventually decrease. Fluid in both cores did end with sulfate concentrations lower than initial concentrations. Iron concentrations in the reservoir for both tests remained very low throughout the experiments, remaining well below concentration levels measured in the back pressure pumps. Over the span of the experiment, iron concentrations in the fluid sampled from cores 5.1, 5.2, 6.1, and 6.2 increased. Barium concentrations for the reservoir in tests 5 and 6 remained higher than concentrations measured in the back pressure pumps. Fluid samples from cores 5.1, 6.1, and 6.2 had an overall increase in barium concentration. Fluid sampled from core 5.2 had a slight decrease in barium during the experiment.

Variability in the fluid chemical concentrations from the back pressure pumps makes geochemical analysis challenging. Decreases in calcium, iron, and barium concentrations noticed in Test 5 were all on the same sampling day (Figure 19). Dilution factors were reevaluated but the calculations appeared to be correct.

From the ICP-OES, ICP-MS, and IC results and from the pH and temperature measurements, mineral saturation indices were calculated using the free geochemical program Visual MINTEQ. Chemical concentrations, pH, and temperature were input into Visual MINTEQ for saturation indices. Oversaturation of minerals were graphed at two time steps for tests 5 and 6 (Figures 21-22). From the mineral saturation indices, barite was slightly over saturated (Figure 21). Hematite remained one of the most over saturated mineral in the back pressure pump fluid for all four cores. Fluid from both cores in test 5 were over saturated in Ferrihydrite.

Discussion

I compared results of different subsets of the experiments to isolate different variables and evaluate effects of time on fluid stability and how variations in mineral composition of the reservoir rock could effect fluid-rock interaction. Comparing CT scan data from the previous tests to my results, I noticed the composition of the Marcellus shale mattered most. The presence of pyrite and calcite in the rock altered fluid pH, chemical species concentrations, mineral saturation indices, and permeability. In these experiments the ammonium persulfate was either not present (tests 5 and 6), or was less reactive (tests 3 and 4) due to a time delay between mixing the fluid and using it. I found that without ammonium persulfate, barite scaling was not an issue despite short time between preparation of the experimental solution and initiation of the experiment. The pH of the hydraulic fracturing fluid with old ammonium persulfate or without ammonium persulfate remained acidic and HCl remained reactive with the Marcellus shale. Without the ammonium persulfate, there may have been a slight decrease in the amount of reaction between the calcite minerals and the HCl.

Effect of Sample Composition Differences on Reaction Area

Using the available data at NETL from tests 3 and 4, and the two tests I completed, I was able to relate physical variations in the rock cores to measured reaction rim fractional area. The two previous tests were completed by Moore et al. (2017) and the CT data were available to my study. A comparison of the results of tests 3, 4, 5, and 6 showed that some physical rock properties, including bedding orientation and mineralogy (composition), influenced the reaction rim area. Test 5 used two cores drilled parallel to bedding, while tests 3 and 4 used cores drilled both perpendicular and parallel to bedding. The amount of calcium carbonate can vary between beds. In test 3, the core drilled perpendicular to bedding had more variation in the amount of reaction than the core drilled parallel to bedding (Figure 18a). From my observations of the CT scans with higher reaction areas coinciding with observed increases in calcite, I inferred that beds with more calcium carbonate reacted more than other beds, creating spikes in the amount of reaction along the fracture. Although test 4 also had cores drilled at different angles with respect to bedding, there did not appear to be as much variation in the reaction relative to bedding direction. Test 4 did have a large difference though in the amount of reaction measured in each core relative to each other, with the core drilled perpendicular to bedding reacting around 20% more (Figure 17b). The difference in the amount of reaction is attributed to variations in the composition of the rock cores. Less calcite in the rock core means there would be less reaction with the HCl. The two cores used in test 5 appeared to have a relatively similar amount of reaction, with the reaction area decreasing further from the inlet. Test 6 had a lack of reaction which coincided with the observed increase of pyrite in the CT scans and along the fracture surface.

Geochemical Reactions inferred from IC and ICP results

In test 5, geochemical reactions not visible in the CT images or in person were identified from mineral saturation indices along with fluid concentrations. The spike in sulfate in core 5.2 fluid could be from pyrite oxidation. The initial spike of sulfate in fluid from core 5.1 could be from residual material in the pipes and pumps from previous experiments. For both cores, precipitation of sulfate minerals was not predicted by the calculated saturation indices (Figure 21). Barium concentrations in cores 5.1 and 5.2 varied throughout the test while the reservoir fluid concentration increased. The decrease in barium concentration from the back pressure pumps, when compared to the reservoir concentration, and a positive saturation value for barite predicts there would be some barite precipitation, although no new barite was directly observed. Both cores also had an increase of calcium and iron in the effluent in comparison to the reservoir, indicating calcium and iron were released into solution from the rock core throughout the test.

In test 6, IC and ICP results were variable, in particular with calcium and iron, and were used in conjunction with saturation indices and comparisons between overall trends. The decrease in calcium and iron concentrations could be from the pump failure experienced on the third day of the test. Without the pump working, fresh fluid with hydraulic fracturing additives would not be flowing through the fracture and reacting with the Marcellus Shale. The decrease in calcium concentration in the reservoir fluid could be due to the small sample sizes collected on the second and fourth day of the test. Dilution factors though were reevaluated but appeared to

be correct. With smaller sample sizes, there might not be enough fluid to accurately depict the fluid chemistry after filtering and dilution. Iron in the reservoir remained low, indicating iron was being released from the rock cores. Although barium levels in the reservoir remained higher than concentrations measured in the effluent, there was not an oversaturation of barite (Figure 22).

Effect of Pyrite Oxidation on pH, Saturation Indices, and Chemical Species Concentrations

Comparing saturation indices and pH between tests 5 and 6, variations between the two tests could be caused by pyrite oxidation. From Tabelin et al. (2017), oxidation of pyrite results in sulfate and H^+ (1).

$$FeS_2 + 3.5O_2 + H_2O \rightarrow Fe^{2+} + 2H^+ + 2SO_4^{2-} \quad (1)$$

This reaction decreases the pH of the fluid which can account for the decrease in pH for test 6 in comparison to test 5 (Figure 14). Sulfate may have remained low due to the high acidity of the reservoir fluid which can slow down pyrite oxidation (Tabelin et al., 2017). Additionally, sulfate forms from a series of intermediate sulfur species which delays the formation of sulfate (Tabelin et al., 2017). From the mineral saturation indices, hematite was one of the most oversaturated mineral in all four core fluids. Tabelin et al. (2017) found that hematite suppressed pyrite oxidation by decreasing the formation of intermediate sulfur species, further limiting sulfate concentrations. In test 5, the saturation indices for hematite were higher than test 6, preventing pyrite oxidation from occurring, allowing the pH to increase in test 5. With a lower saturation of hematite, less calcite in the core, and more pyrite in the core, the pH level in test 6 would have decreased and would not be buffered from calcite dissolution. Ferrihydrite was an additional mineral oversaturated in test 5 which could indicate there was some pyrite oxidation. Calcite dissolution can neutralize acidic fluids and prevent an increase in acidity from pyrite oxidation (Chermak et al. 2014). From Chermak et al. (2014), pyrite oxidation and calcite dissolution can be combined (2). The result is sulfate and ferrihydrite in a less acidic fluid.

$$FeS_2 + 4CaCO_3 + 15/4O_2 + 7/2H_2O \rightarrow Fe(OH)_3 + 2SO_4^{2-} + 4Ca^{2+} + 4HCO_3^- \quad (2)$$

Comparison of Reaction Area to Changes in pH Between the Reservoir and the Effluent

The acidity of the synthetic hydraulic fracturing fluid did not appear to be the decisive factor in the amount of calcite dissolution along the fracture surface. Test 3 had the highest reaction percent and the reaction appeared to be relatively stable throughout the cores (Figure 17a). Interestingly, the pH of the fracturing fluid for test 3 was the least acidic of all the tests (Figure 15). Additionally, the effluent from test 3 was the most neutral (Figure 15). In tests 3, 4, and 5 the fluid became less acidic due to the buffering effect of the HCl reacting with the calcite minerals. Over the span of the three experiments, the buffering effect did appear to decrease. The pH of the effluent in all three tests were slightly higher from the B2 sampling site than B1. This may suggest some variation between the two fluid flow systems or from sampling methods.

Both cores in test 4 had a consistent amount of reaction throughout the length of the cores but the amount of reaction measured was very different between the two cores. The core drilled

perpendicular to bedding (4.2) appeared to have a similar amount of surface dissolution as test 3 while the core drilled parallel to bedding (4.1) was around 20% less reactive (Figure 17b). The hydraulic fracturing fluid used in test 4 as well as the effluent were the most acidic out of all the tests (Figure 15). Core 4.1 had a significantly lower amount of reaction but the effluent pH was only slightly lower than core 4.2. With the same fluid flowing through both cores, I would have expected the lower reaction in core 4.1 to have a much lower pH when considering the buffering effect from calcite dissolution. The amount of calcite in the two cores could have been different, with both having enough calcite to have a buffering effect. Additionally, there may have been a high enough ratio of calcite to pyrite in core 4.1 to increase the pH.

A major difference between the four tests was the lack of ammonium persulfate in tests 5 and 6. Ammonium persulfate is usually added to break down the gelling agent used to prevent proppant from falling out of suspension during fracturing (Al-Muntasheri, 2014). For tests 5 and 6 the ammonium persulfate was omitted of the synthetic fracturing fluid to more closely resemble the hydraulic fracturing fluid used in the MSEEL project. The change in the fracturing fluid composition may account for the difference in reaction area for test 5 in comparison to tests 3 and 4. The fractional area of the fracture that reacted in test 5 was around 0.35 and 0.4 while test 4 was around 0.6 and 0.8 (Figures 17b and 18). The guar gum and gelling agent remained intact without the ammonium persulfate present to break down the gelling agents in the fluid, potentially prevented the HCl from reacting with the calcite because the more viscous fluid may have coated the rock surface. Another possibility: as the HCl became more neutralized away from the inlet, the acid was not strong enough to have as much of a reaction towards the outlet.

Physical Characteristics Observed in Computed Tomography Images of Test 5

Fracture roughness appears to influence the volume of host rock that reacts with the fluid. From the post-reaction CT images for test 5 and the plotted reaction volume, potentially interesting sections of high and low reaction were investigated further. Around halfway along the length of the core, the reaction volume drops to under 0.05 mm^3 (Figure 18). From the post CT images, the fracture in this section becomes very straight and smooth (Figure 23). In comparison the reaction volume around 31.5 mm peaks and in the CT images the fracture has a more irregular profile and the reaction rim is visibly thicker, particularly on the right side (Figure 24).

Proppant placement may influence the amount of reaction along the fracture. The amount of proppant remained relatively low for both cores in test 5. On the bottom half of core 5.1, there are two spikes in proppant around 20 mm and 34 mm (Figure 16a). The amount of reaction is also higher at these two points along the core. While the reaction increases and decreases without significant changes in the proppant volume, where the proppant is concentrated, there is a higher amount of reaction. The bottom half of core 5.2 did not appear to have easily identifiable relationships between proppant location and the reaction rim thickness (Figure 16b). Depressurizing and moving the core from the fluid flow system to the industrial scanner may have moved proppant, causing a loss in data.

A combination of proppant placement and increased calcite concentration caused the right side, when looking down the length of the core from the inlet, of core 5.2 to react more. Proppant prevents the fracture from closing but it can also alter the flow path of the fluid. The

lack of proppant on the left side allowed the fracture to narrow, reducing the amount of flow and thereby the degree the fracture surface could react. Unfortunately, due to depressurizing the sample to be scanned after the test, a conclusive analysis of the proppent's impact on the location and amount of reaction cannot be made. With fluid flowing on the right side of the core, the increased amount of calcite on the right side could easily react. Closer to the outlet, large conical calcite pieces intersecting the fracture are visible, propagating further away from the fracture surface (Figure 13). The fracture roughness also appeared to influence the amount of reaction. A smoother fracture surface had less reaction when compared to a rougher fracture surfaces (Figure 24).

The presence of pyrite in the Marcellus Shale can also influence fluid-rock interaction. The reaction volume vs. distance along the length of the core sharply drops at ~ 5 mm from the inlet of the core before quickly increasing again (Figure 16b). Reviewing the corresponding core images, there is a concentration of highly attenuated pyrite nodules throughout the core (Figure 25). Pyrite indicates the depositional environment was more acidic, decreasing the amount of calcite being deposited (Roberts, Walker, and Buchanan, 1969; Krumbein and Garrels, 1952; Reineck and Singh, 1975). With more pyrite there should be less calcite in this section of the core, which corresponds with the lack of visible calcite dissolution. The only visible dissolution is along a calcite vein.

Findings and Recommendations

For tests 3 and 4, the fracturing fluid was mixed up to three weeks before use, while the fluid for test 5 was mixed an hour before use. Despite the time difference, all three tests had very similar pH buffering reactions. The hydrochloric acid did not appear to degrade over time, even with ammonium persulfate present in tests 3 and 4. In comparison, in test 6, pH buffering did not occur to the same degree as earlier tests. The only variation between tests 5 and 6 was the rock cores used. The composition of the rock cores was the controlling factor in fluid-rock reactions.

Mineralogical changes appeared to have a greater impact on the local effectiveness of the fracturing fluid to increase permeability than proximity to the inlet. From core 2 in test 5, a section of the core close to the inlet had high concentrations of pyrite and low concentrations of calcite causing the reaction rim volume to drop. Comparing tests 5 and 6, fracture reaction can be related to Marcellus Shale composition. The two tests used the same hydraulic fracturing fluid and the fluid was mixed at about the same time before each test. The only difference between the two tests was the Marcellus Shale rock cores. Test 6 cores had more pyrite visible along the fractures and throughout the cores. With more pyrite present, there is less calcium carbonate present to react with the hydraulic fracturing fluid. Given these findings, I would recommend further studies to identify at what scale compositional variations begin to impact production. A comparison of results from experiments along the length of the MSEEL core relative to rock core composition could provide information on an applicable scale for the hydraulic fracturing industry. Identifying at what scale mineral variation will begin to have an impact on production could alter the length of the section of the horizontal well that is fractured and shut-in.

Barite precipitation did not occur in these experiments, despite conditions in which barite precipitation was expected: fresh hydraulic fracturing fluids, shut-in for five days. None of the

four different Marcellus Shale rock cores showed barite precipitation, and (as argued above) they varied in composition. The lack of barite precipitation is consistent with the findings of Hakala et al. (2017), despite the change in time between mixing the hydraulic fracturing fluid and using the fluid. However, in contrast to the Hakala et al. (2017) study, the hydraulic fracturing fluid used in tests 5 and 6 reported here lacked ammonium persulfate. With little to no ammonium persulfate, there is not enough sulfate for barite to precipitate. I infer that the lack of ammonium persulfate is the critical difference, rather than the difference in time between mixing and using the hydraulic fracturing fluid.

In September of 2017, an additional test, test 7, comparing temporal variations in preparing hydraulic fracturing fluid that contains ammonium persulfate was completed. Comparing tests 5 and 6 against test 7 will verify if ammonium persulfate is a main contributor to barite scale formation. Comparing test 7 against tests 3, 4, 5, and 6 will provide data on the temporal decay of the fracturing fluid with ammonium persulfate and how fresh ammonium persulfate will alter fluid-rock interactions.

References Cited

Al-Muntasheri, G., 2014, A critical review of hydraulic fracturing fluids over the last decade, in Society of Petroleum Engineers Western North American and Rocky Mountain Joint Regional Meeting: Denver, Colorado, SPE 169552.

Atkinson, D., Smelser, R. E., and Sanchez, J., 1982, Combined mode fracture via the cracked Brazilian disk test: International Journal of Fracture, v. 18(4), p. 279-291.

Chermak, J. A., and Schreiber, M. E., 2014, Mineralogy and trace element geochemistry of gas shales in the United States: Environmental implications: International Journal of Coal Geology, v. 126, p. 32-44.

Clark, S. H. B., Birth of the mountains: The geologic story of the southern Appalachian Mountains, USGS: https://pubs.usgs.gov/gip/birth/birth.pdf (accessed August 2017).

Donaldson, E. C., Alam, W., and Begum, N., 2013, Hydraulic fracturing explained: evaluation, implementation, and challenges: Houston, Gulf Publishing Company, 194 p.

Energy Information Administration, Natural Gas Explained: Where Our Natural Gas Comes From: https://www.eia.gov/energyexplained/index.cfm?page=natural_gas_where (accessed July 2017).

Energy Information Administration, 2017, Marcellus Shale Play: Geology review: https://www.eia.gov/maps/pdf/MarcellusPlayUpdate_Jan2017.pdf

Fakcharoenphol, P., Torcuk, M., Kazemi, H., and Wu, Y., 2016, Effect of shut-in time on gas flow rate in hydraulic fractured shale reservoirs: Journal of Natural Gas Science and Engineering, v. 32, p. 109-121.

Ferrar, K.J., Michanowicz, D.R., Christen, C.L., Mulcahy, N., Malone, S.L., and Sharma, R.K., 2013, Assessment of effluent contaminants from three facilities discharging Marcellus shale wastewater to surface waters in Pennsylvania: Environmental Science & Technology, v. 47, p. 3472-3481.

Hakala, J., Crandall, D. Moore, J., Phan, T., Sharma, S., and Lopano, C., 2017, Laboratory-scale studies on chemical reactions between fracturing fluid and shale core from the Marcellus Shale energy and environmental laboratory (MSEEL) site, in Unconventional Resources Technology Conference: Austin, Texas.

Harper, J. A., and Kostelnik, J., The Marcellus Shale play in Pennsylvania: Part 2: Basic geology, Pennsylvania Department of Conservation and Natural Resources: http://www.docs.dcnr.pa.gov/cs/groups/public/documents/document/dcnr_007593.pdf (accessed September 2017).

Hodge, T., 2016, Natural gas expected to surpass coal in mix of fuel used for U.S. power generation in 2016: Today in Energy, U.S. Energy Information Administration: https://www.eia.gov/todayinenergy/detail.php?id=25392 (accessed July 2017).

Krumbein, W. C., and Garrels, R. M., 1952, Origin and classification of chemical sediments in terms of pH and oxidation-reduction potentials: The Journal of Geology, v. 60(1), p. 1-33.

Liu, N., Liu, M., and Zhang, S., 2015, Flowback patterns of fractured shale gas wells: Natural Gas Industry B, v. 2, p. 247-251.

Lutz, B.D., Lewis, A.N., and Doyle, M.W., 2013, Generation, transport, and disposal of wastewater associated with Marcellus Shale gas development: Water Resources Research, v. 49(2), p. 647-656.

Milici, R. C., and Swezey C. S., 2006, Assessment of Appalachian Basin oil and gas resources:

Devonian Shale-Middle and Upper Paleozoic total petroleum system: USGS, U.S. Department of the Interior: https://pubs.usgs.gov/of/2006/1237/ (accessed October 2017).
Moore, J., Hakala, A., Vankueren, A., Phan, T., and Crandall, D., 2017, Experiments evaluating geochemical alteration of matrix materials adjacent to simulated hydraulic fractures, in Proceedings, GSA Joint 52nd Northeastern Annual Section/ 51st North-Central Annual Section Meeting, March 19 2017: Geological Society of America Abstracts with Programs, Vol. 49, No. 2.
Marcellus Center for Outreach and Research, Pennsylvania State University, no date. Depth to Marcellus Shale Base: Maps and Graphics: http://www.marcellus.psu.edu/resources-maps-graphics.html (accessed October 2017).
Marcellus Center for Outreach and Research, Pennsylvania State University, no date. Thickness of Marcellus Shale: Maps and Graphics: http://www.marcellus.psu.edu/resources-maps-graphics.html (accessed October 2017).
Orem, W., Tatu, C., Varonka, M., Lerch, H., Bates, A., Engle, M., Crosby, L., and McIntosh, J., 2014, Organic substances in produced and formation water from unconventional natural gas extraction in coal and shale: International Journal of Coal Geology, v. 126, pp. 20-31.
Reineck, H., and Singh, I. B., 1973, Depositional sedimentary environments: with reference to terrigenous clastics: Berlin, New York, Springer-Verlag, 439 p.
Renock, D., Landis, J.D., and Sharma, K., 2016, Reductive weathering of black shale and release of barium during hydraulic fracturing: Applied Geochemistry, v. 65, p. 73-86.
Roberts, W. M. B., Walker, A. L., and Buchanan, A. S., 1968, The chemistry of pyrite formation in aqueous solution and its relation to the depositional environment: Mineralium Deposita, v. 4, p. 18-29.
Stair, C., Ghosh, S., and Jackson, R., 2017, MSEEL Project Context: State of the Region (2001-2014), Regional Research Institute West Virginia University: http://rri.wvu.edu/wp-content/uploads/2017/01/Resource_Doc2017-01-1.pdf (accessed August 2017).
Stringfellow, W. T., Domen, J. K., Camarillo, M. K., Sandelin, W. L., and Borglin, S., 2014, Physical, chemical, and biological characteristics of compounds used in hydraulic fracturing: Journal of Hazardous Materials, v. 275, p. 37-54.
Tabelin, C. B., Veerawattananun, S., Ito, M., Hiroyoshi, N., and Igarashi, T., 2017, Pyrite oxidation in the presence of hematite and alumina: I. Batch leaching experiments and kinetic modeling calculations: Science of the Total Environment, v. 580, p. 687-698.
USGS, Geologic provinces of the Unites States, Appalachian highlands province, Geology and National Parks: https://geomaps.wr.usgs.gov/parks/province/appalach.html (accessed October 2017).
Vankeuren, A. N. P., Hakala, J. A., Jarvis, K., and Moore, J. E., 2017, Mineral reactions in shale gas reservoirs: Barite scale formation from reusing produced water as hydraulic fracturing fluid: Environmental Science & Technology, v. 51, p.9391-9402.
Wang, G., and Carr, T., 2012, Methodology of organic-rich shale lithofacies identification and prediction: A case study from Marcellus Shale in the Appalachian basin: Computers & Geosciences, v. 49, p. 151-163.

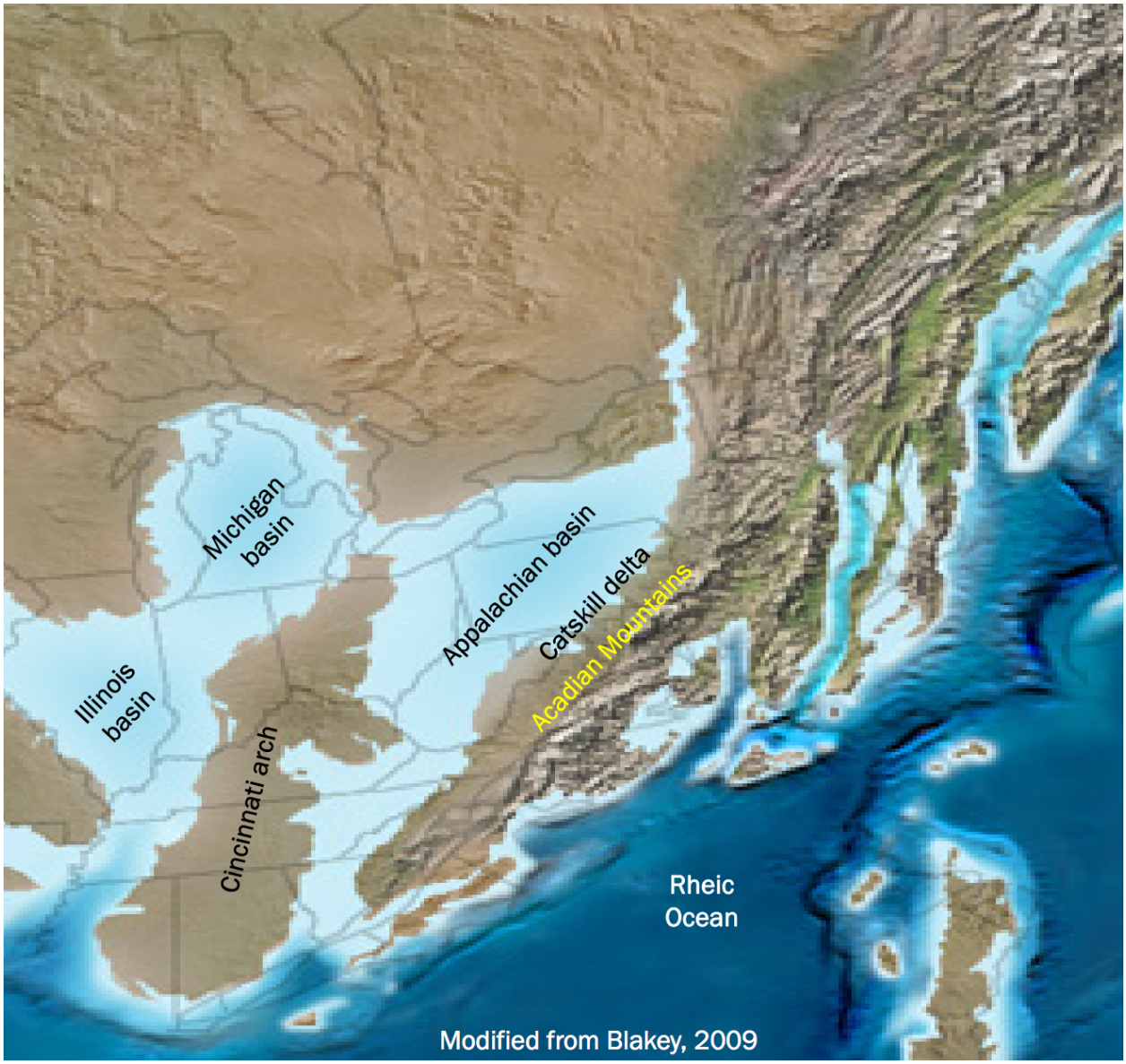

Figure 1: Map of the Appalachian Basin, Catskill delta, Acadian Mountains, and the Rheic Ocean. Blakey (2009) in Harper and Kostelnik (accessed September 2017).

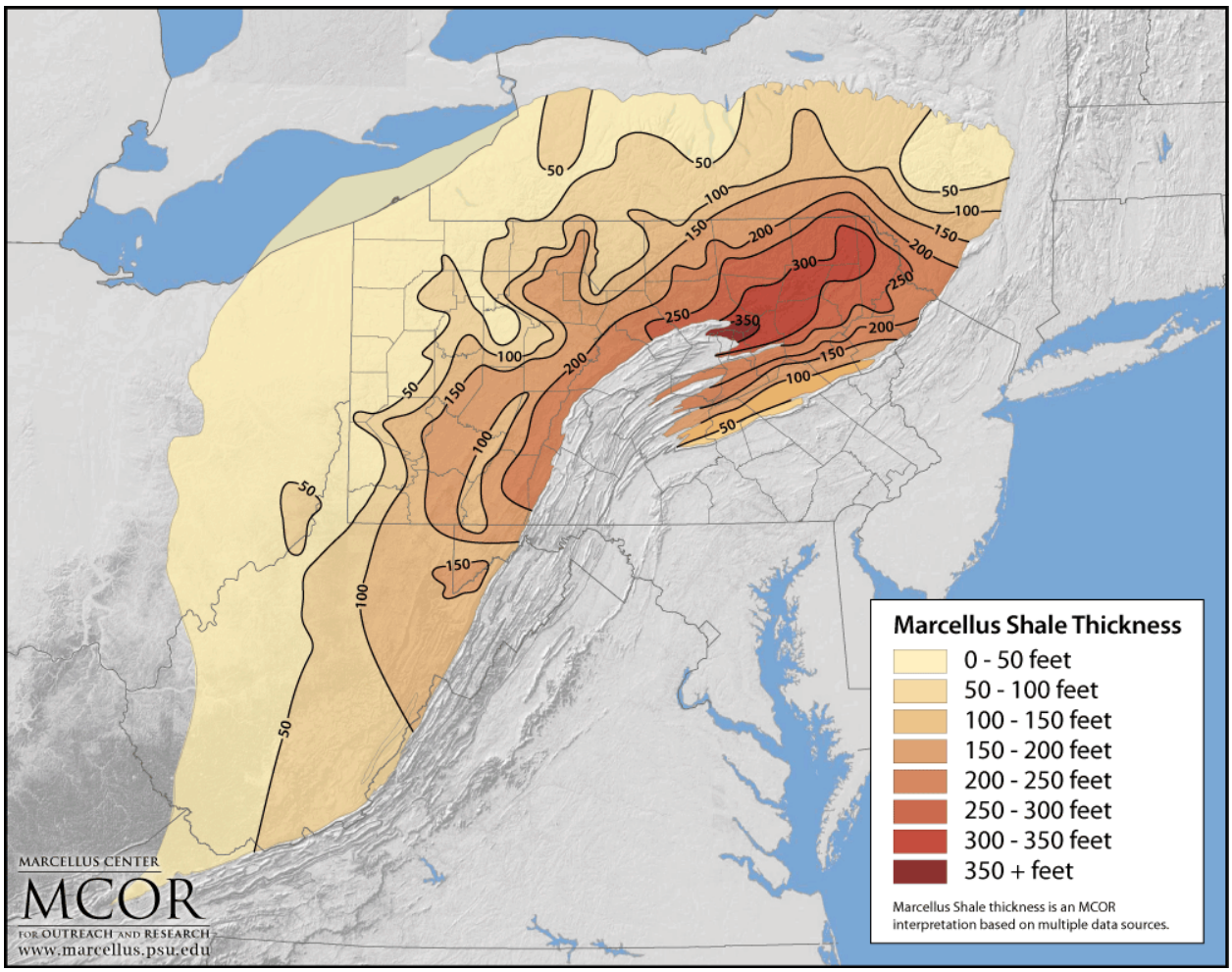

Figure 2: Estimated thickness of the Marcellus Shale. The Marcellus Shale is thickest near the Appalachian Mountains. Figure from Pennsylvania State Marcellus Center for Outreach and Research (Accessed October 2017).

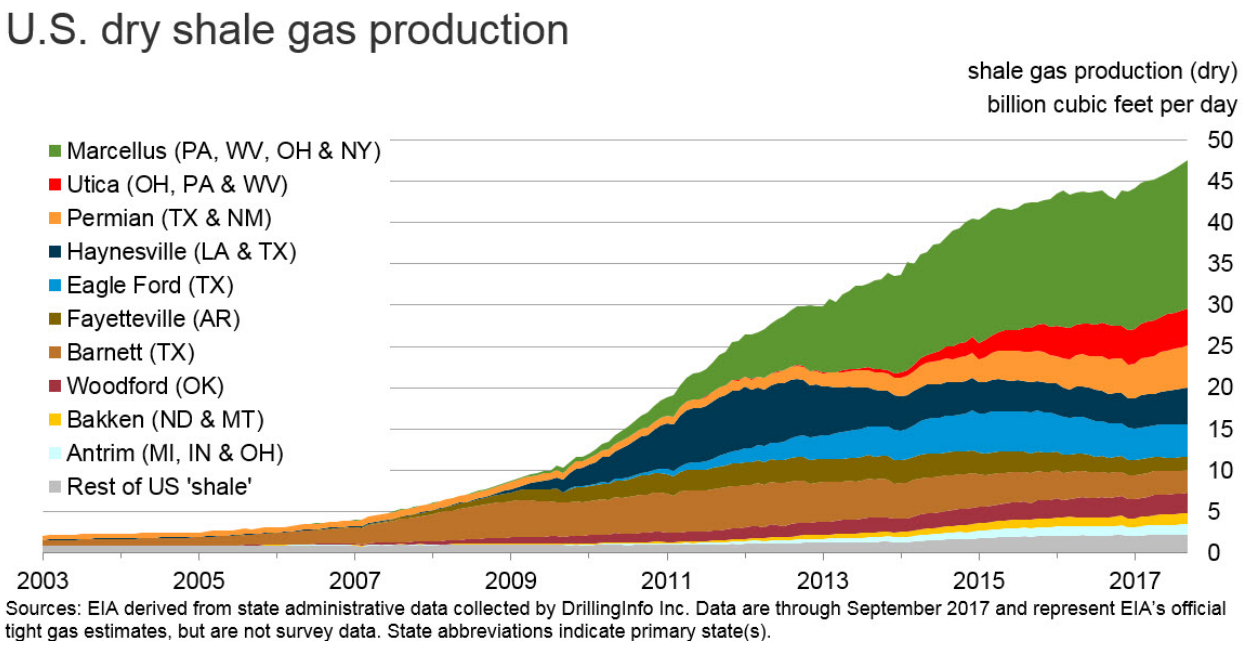

Figure 3: EIA dry shale gas production estimates from 2003 to 2017. The Marcellus Shale (in green) has rapidly increased production and currently is the most productive US dry shale unit. (Energy Information Agency, 2017, Natural Gas Explained).

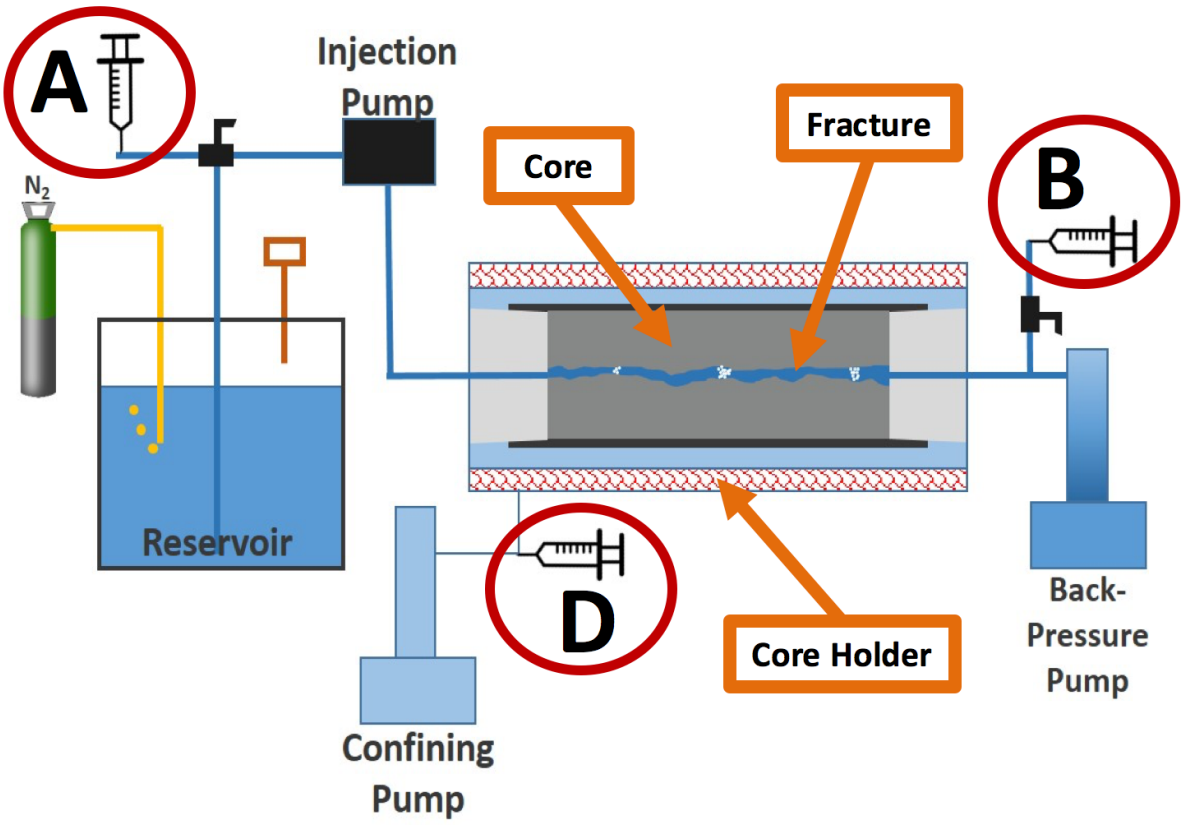

Figure 4: Figure of the fluid flow system used at the National Energy Technology Lab in Morgantown, WV. Daily sampling was taken from the reservoir (A) and from the back-pressure pumps (B). Samples were taken on the first and last day from the confining pumps (D). Adapted from Hakala, et al. (2017).

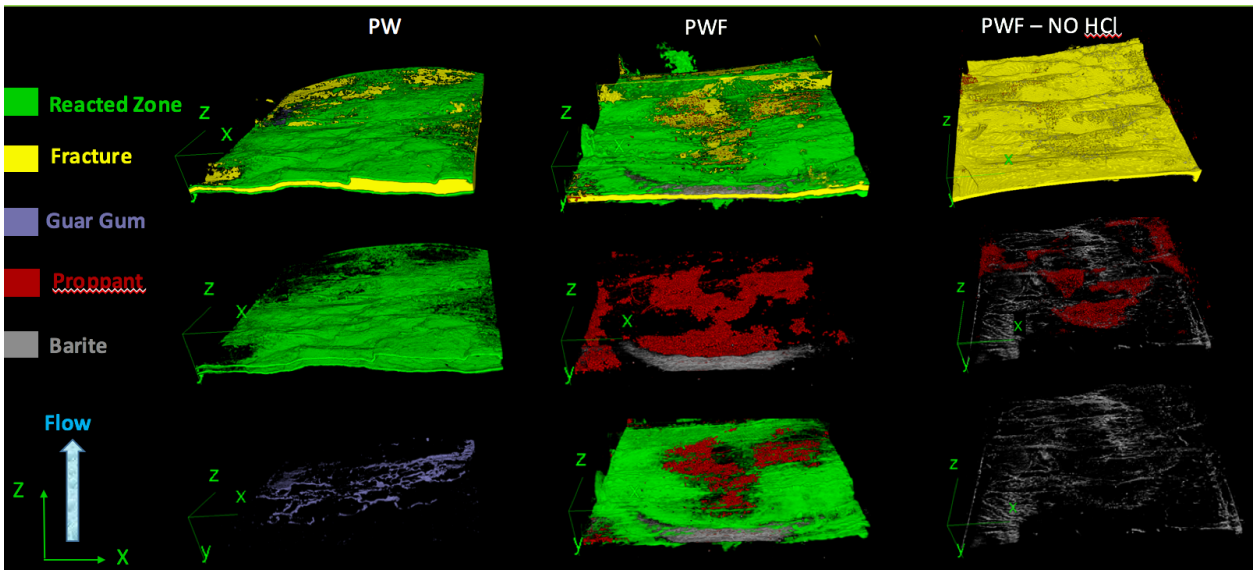

Figure 5: Comparison of CT images of Marcellus Shale cores from experiments by Vankeuren et al. with synthetic reused produced water (PW), synthetic reused produced water with hydraulic fracturing fluid chemicals added (PWF), and synthetic reused produced water with hydraulic fracturing fluid chemicals added without hydrochloric acid added (PW – NO HCL) (Vankeuren et al., 2017). Without fresh chemicals added, guar gum remained intact. With hydrochloric acid present, calcite reacted and dissolved into the fluid. Image from Moore et al., 2017.

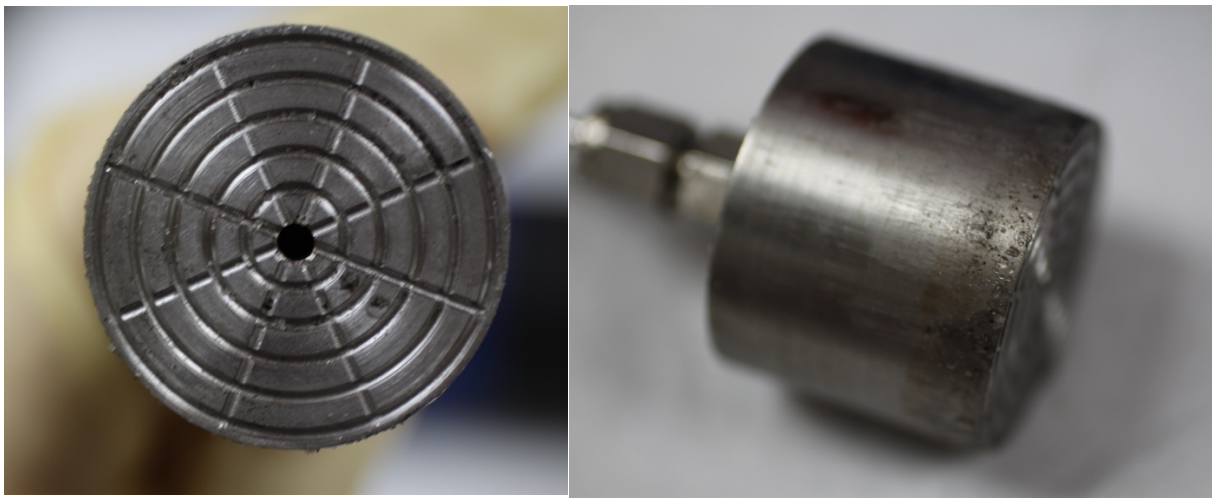

Figure 6: Image of one of the end bells used to hold the cores in place in the Buna-N rubber tubes. The hole in the middle and the etchings delivers the fluid to the front end of the core. An identical end bell is placed at the end of the core. Image by Johnathan Moore, 2017.

Figure 7: Image of one of the Buna-N rubber tubes used in both tests. Rubber tubes were used due to their lower attenuation for CT scanning than metal casings. Image by Johnathan Moore, 2017.

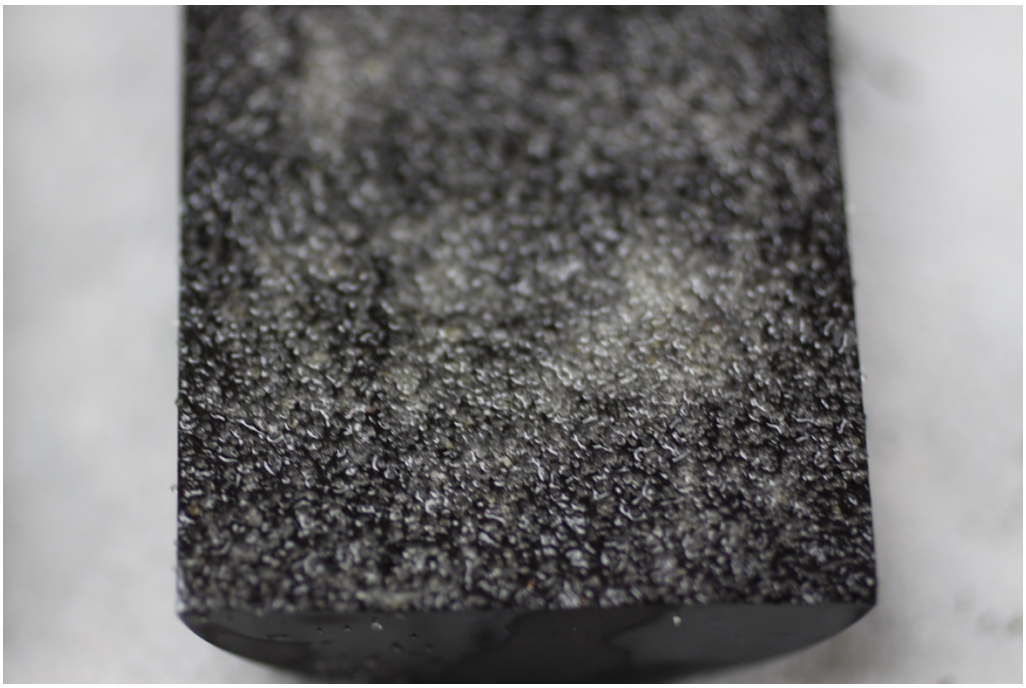

Figure 8: Image of one of the cores with proppant applied to the fresh fracture. Image by Johnathan Moore, 2017.

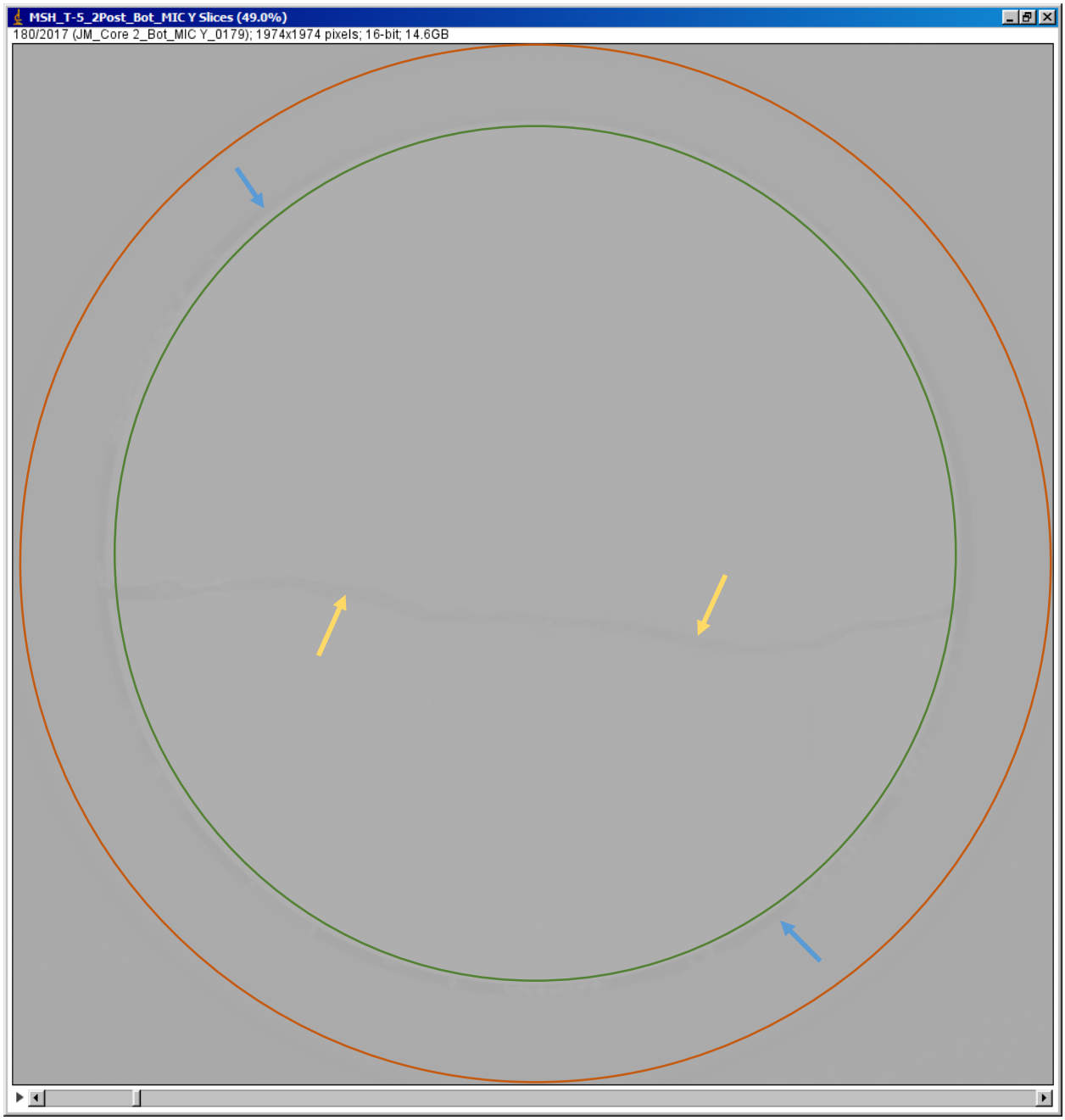

Figure 9: The core is somewhat visible with the horizontal fracture (indicated in yellow). From the center of the image there is the core (circled in green), then a small amount of air (indicated in blue), the rubber casing (circled in orange), and then air.

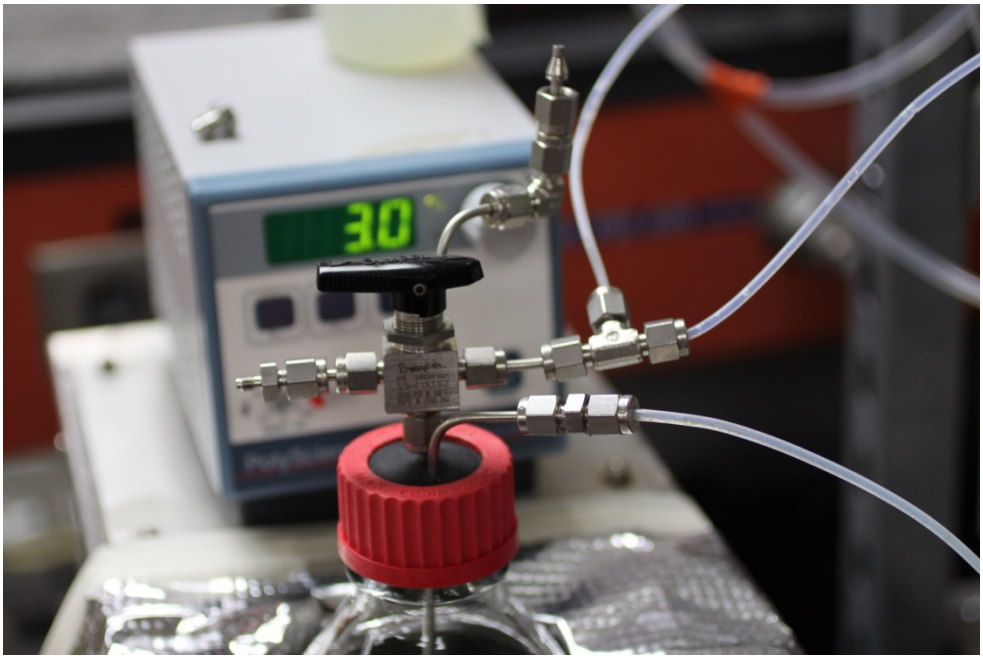

Figure 10: The top of the beaker holding the synthetic fracturing fluid. The top metal valve released gas as pressure built up. The top two plastic tubes fed the synthetic fracturing fluid to both pumps, which then pumped the fluid into both cores. Nitrogen gas was fed into the beaker through the bottom plastic tube. Image by Johnathan Moore, 2017.

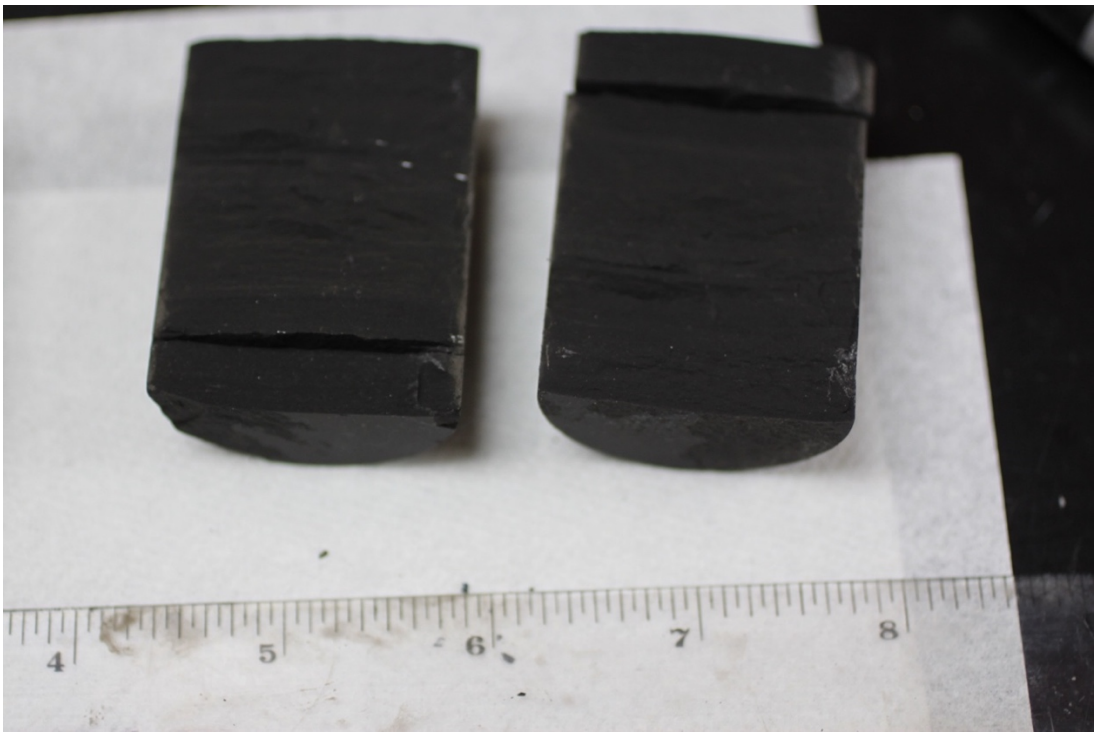

Figure 11: Image of a 1.5” Marcellus Shale core after fracturing. Image by Johnathan Moore, 2017.

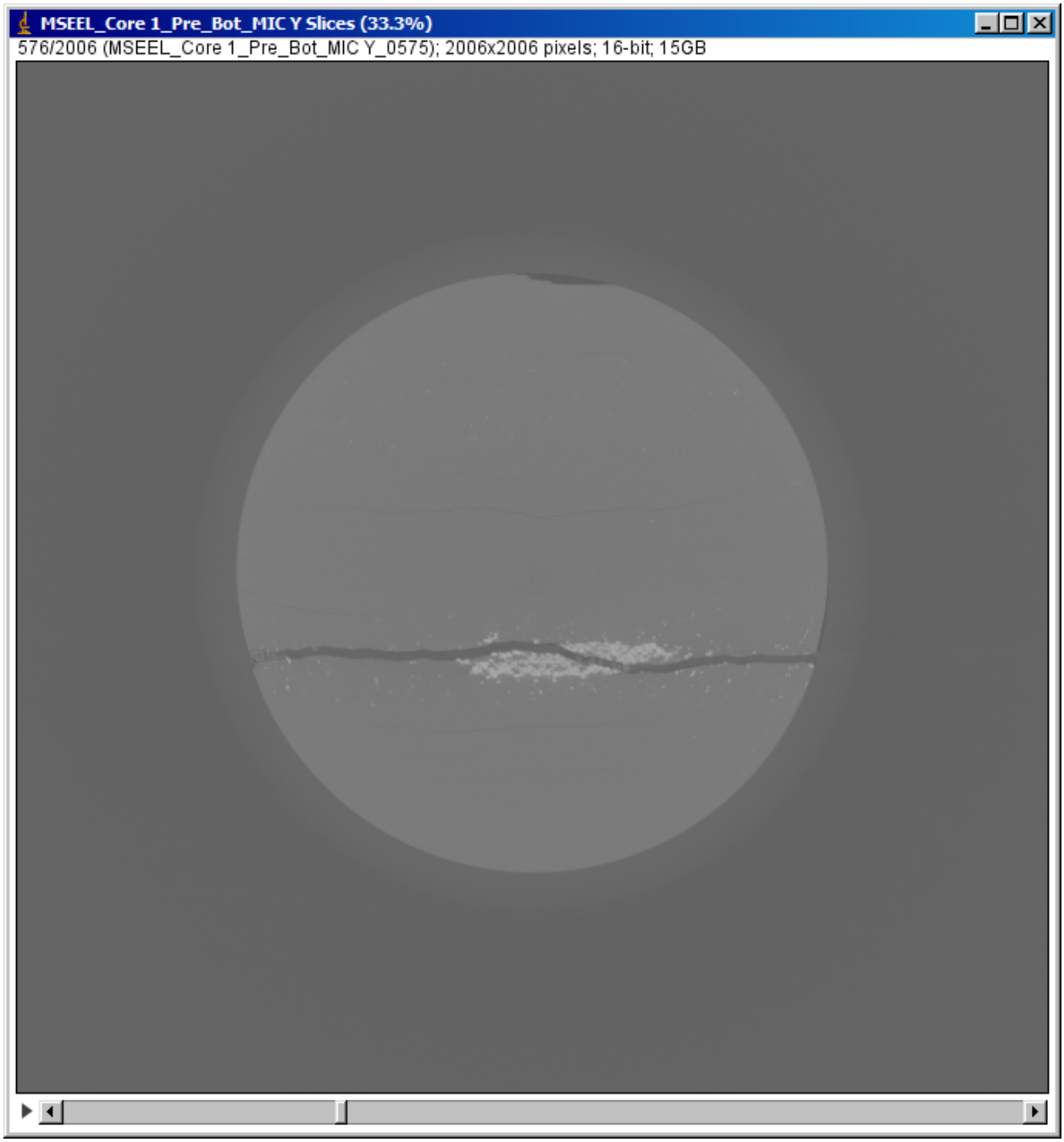

Figure 12: ImageJ image of the MSEEL core samples before test 6. The highly attenuating framboidal pyrite appears as a bright white in the scans. In this example image, pyrite was concentrated in a thin layer where the rock naturally fractured.

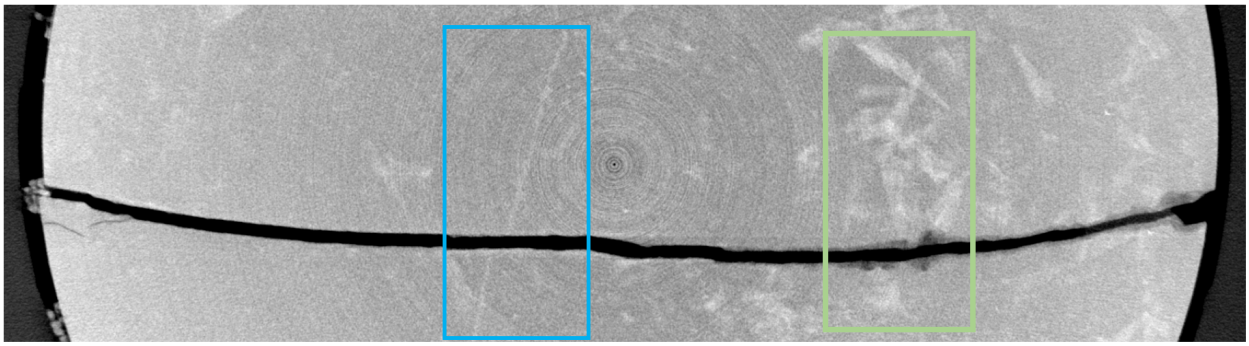

Figure 13: From the bottom of core 5.2, slice number 1374 (around 32.01 mm) shows the dissolution of calcite intersecting the fracture (dark grey), boxed in green. An example of a calcite vein is boxed in blue.

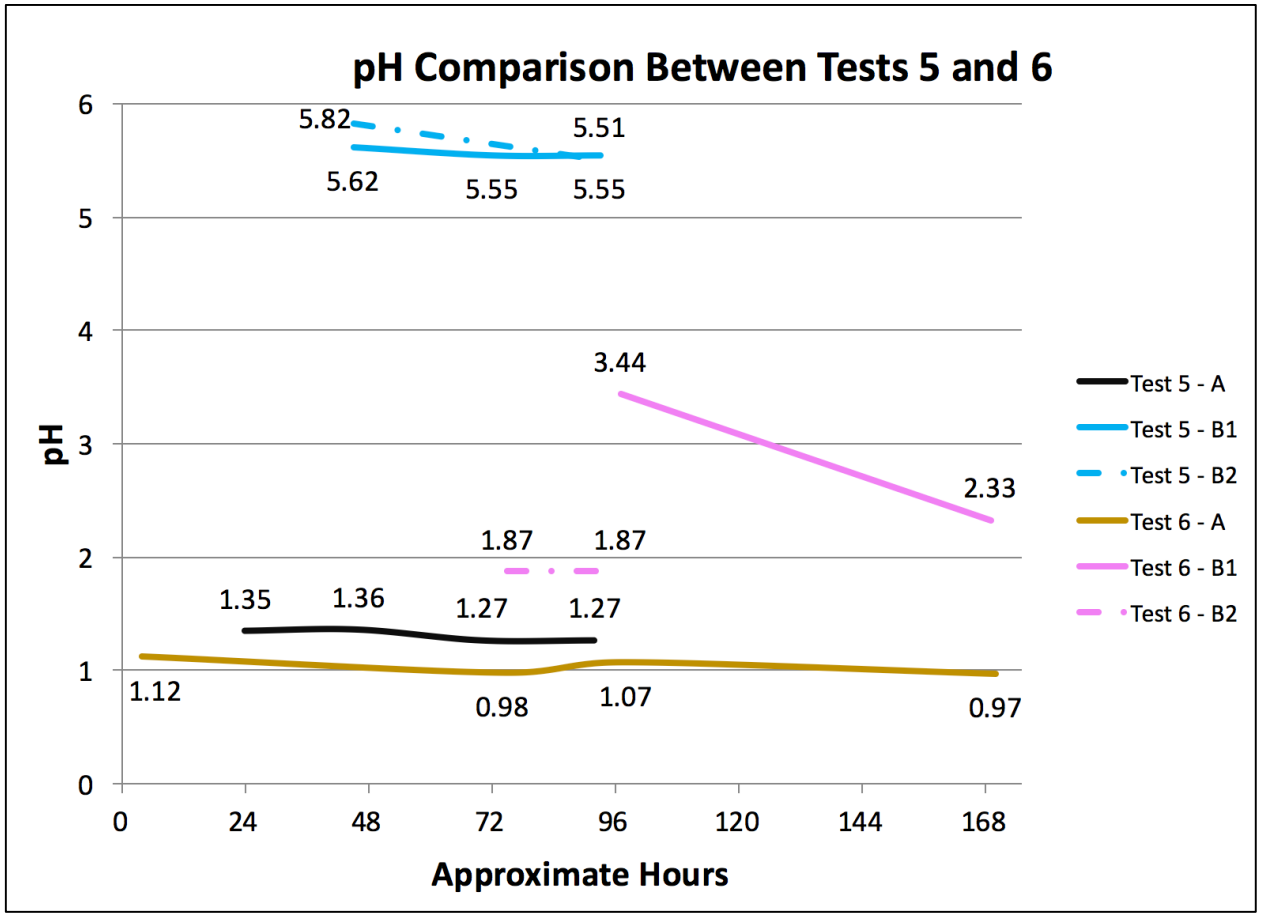

Figure 14: pH of fluid sampled from the reservoir (location A) and from the back pressure pumps (locations B1 and B2) for tests 5 and 6. At sampling location A, the pH for test 5 (black) and test 6 (gold) remained relatively stable and acidic throughout the duration of the tests. Test 6 was extended due to a pump failure. At sampling location B, test 5 (light blue) was more neutral with a slight decrease in pH over the span of the test. At sampling location B for test 6 (light pink), the pH varied between the two cores. Core 2 (dashed line) remained stable but acidic. Core 1 (solid line) became more acidic over time.

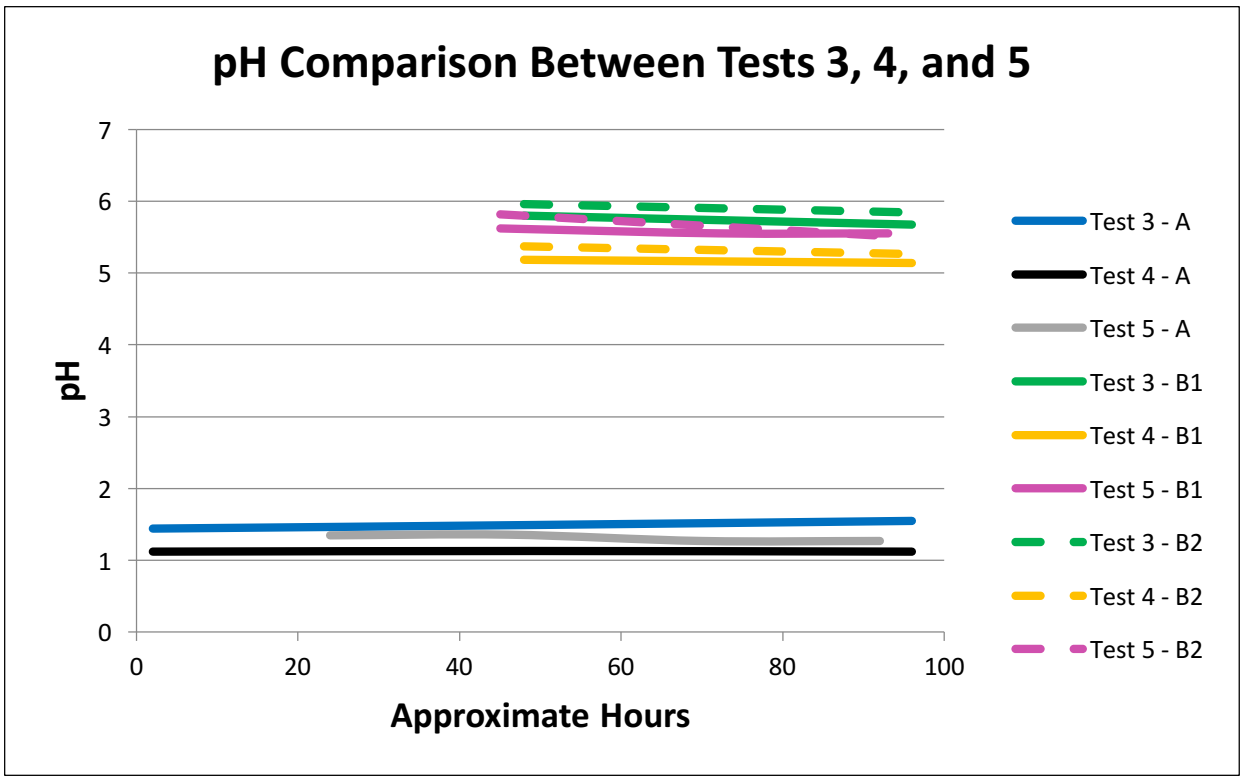

Figure 15: Graph showing tests 3, 4, and 5 pH results. The reservoir, sample point A, remained acidic throughout for all three tests. Fluid from sample sites B1 and B2 for all three tests were all more neutral with a similar pH. In each test B2 (dashed lines) was slightly more neutral than B1 (solid lines).

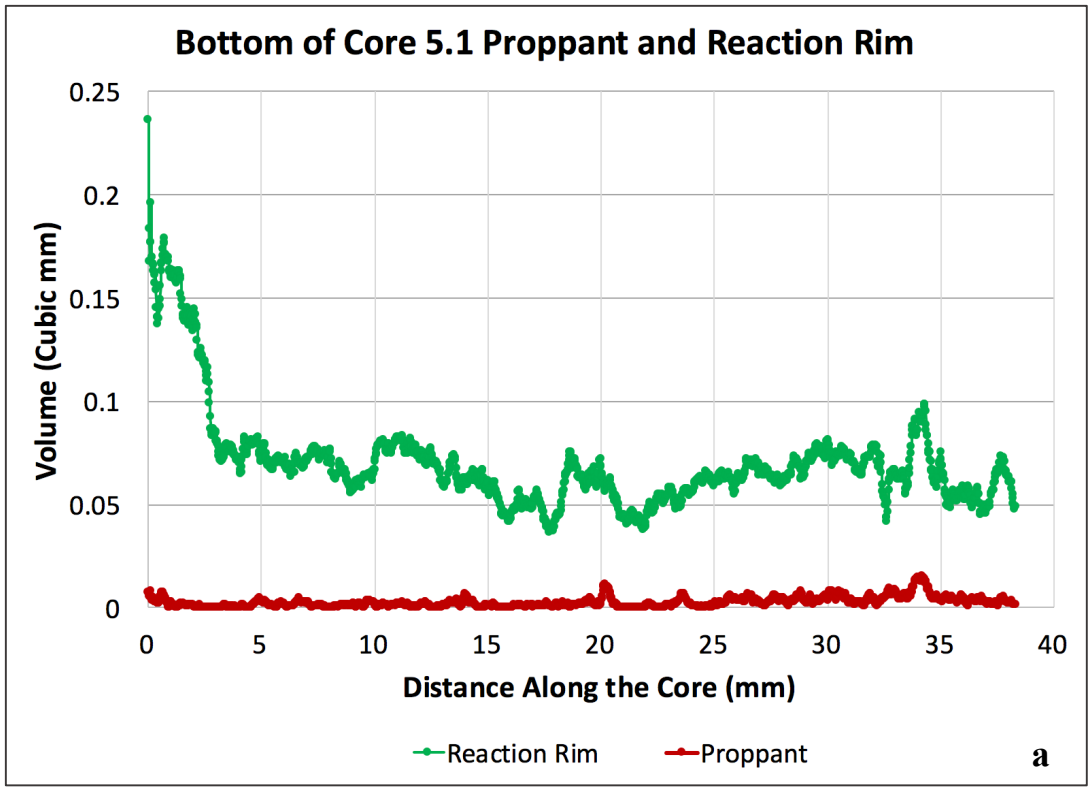

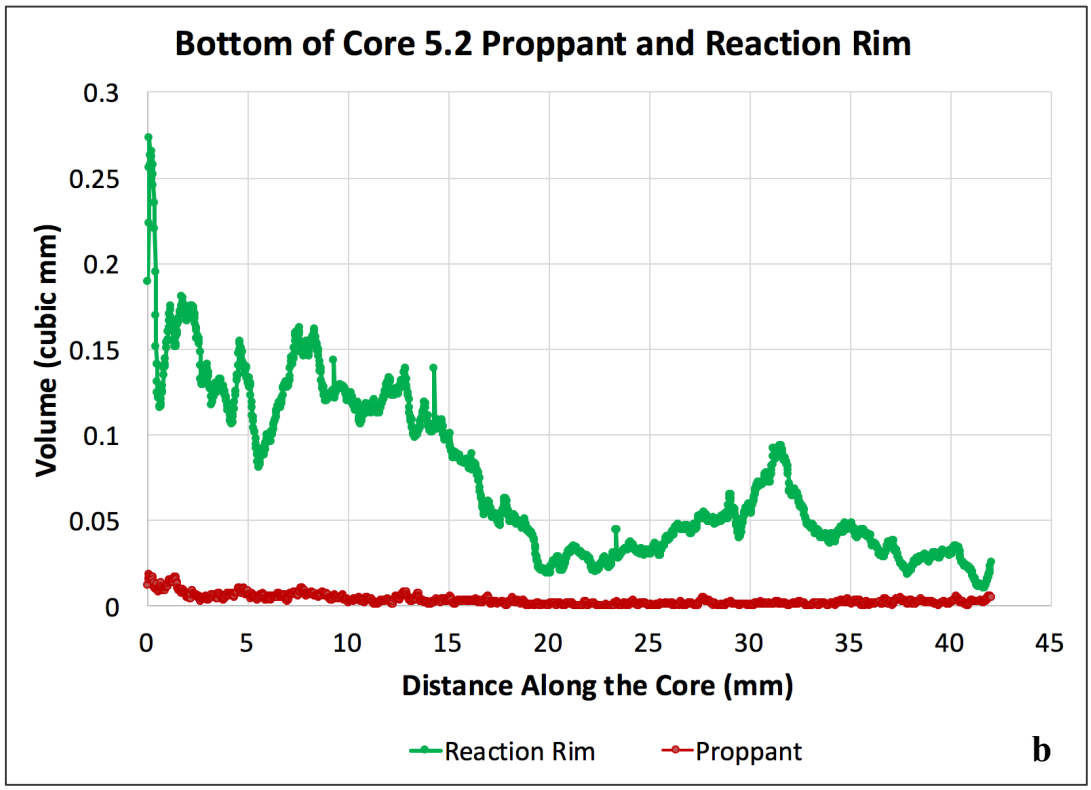

Figure 16: The volume of the reaction rim (green) and the proppant (red) through the length of the bottom half of cores 5.1 (a) and 5.2 (b). The fluid inlet was at 0mm where the reaction rim volume is highest. At around 20 mm and 34 mm from the inlet for core 5.1, there are spikes in the amount of proppant.

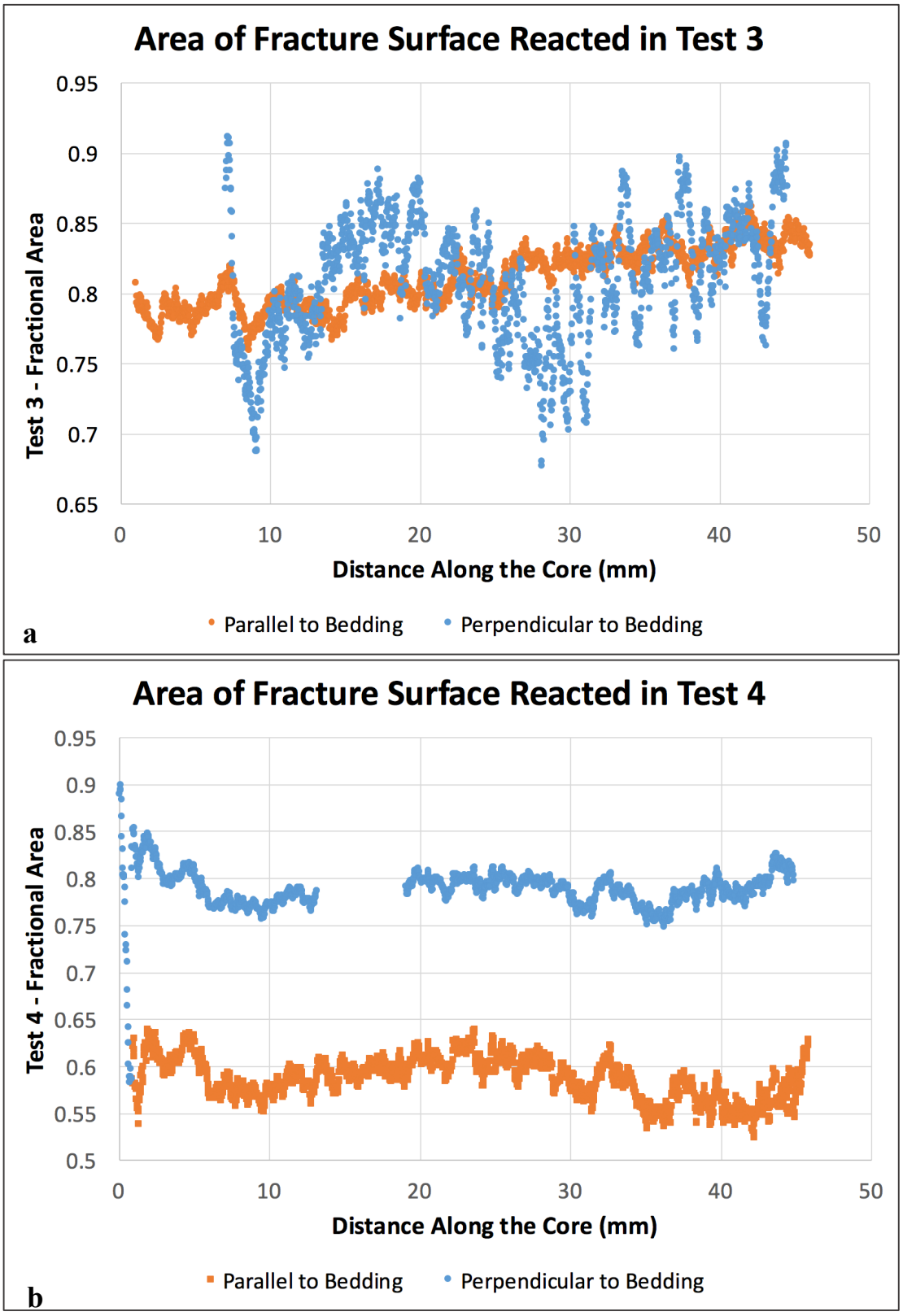

Figure 17: Tests 3 (a) and 4 (b) with one core drilled parallel to bedding (orange) and the second core drilled perpendicular to bedding (blue). In test 4, there is around a 20% difference in the area of the fracture that reacted between the two cores.

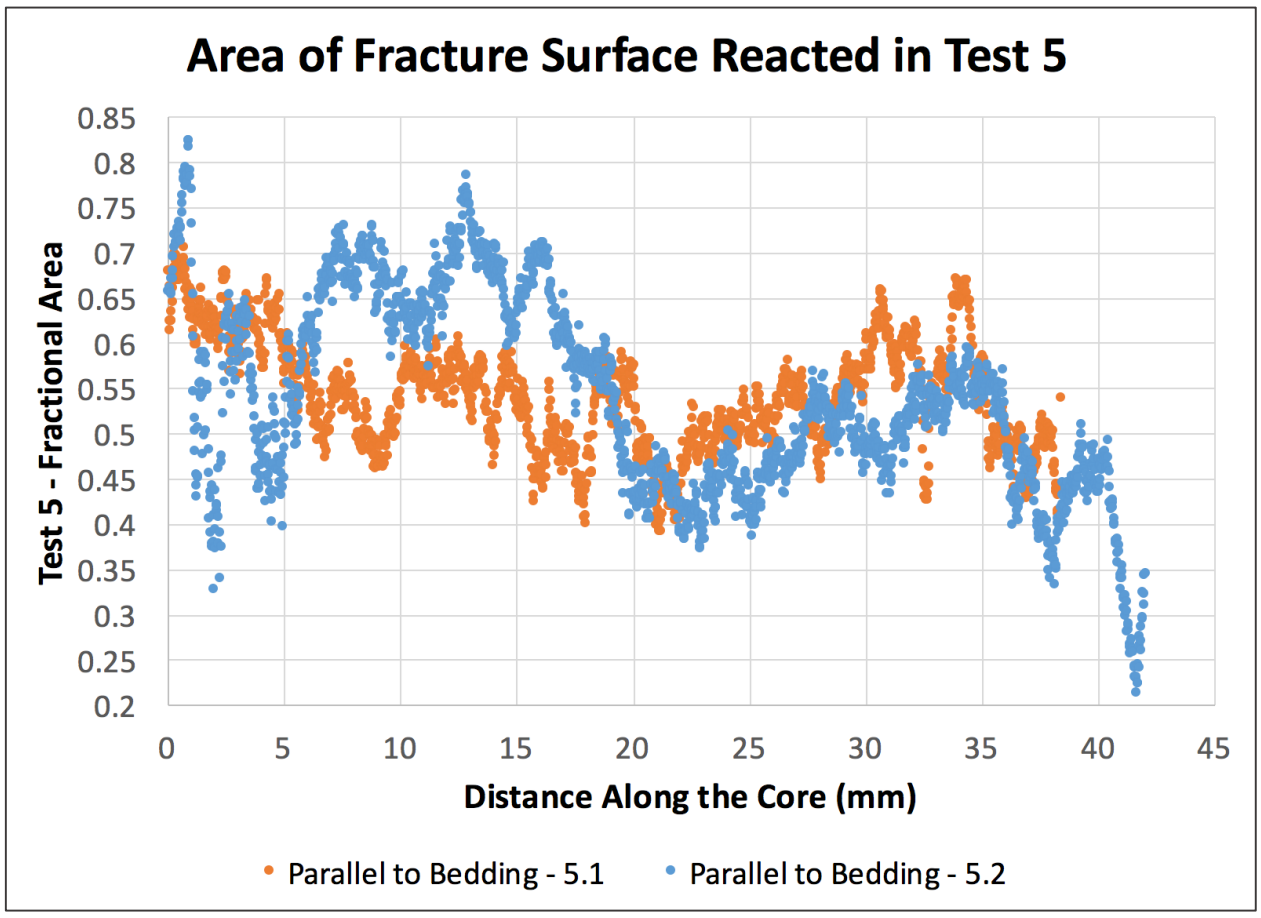

Figure 18: In test 5 the reaction along the fracture was more variable when compared to tests 3 and 4. Both cores were drilled parallel to bedding. Overall both cores decreased in reaction further away from the inlet.

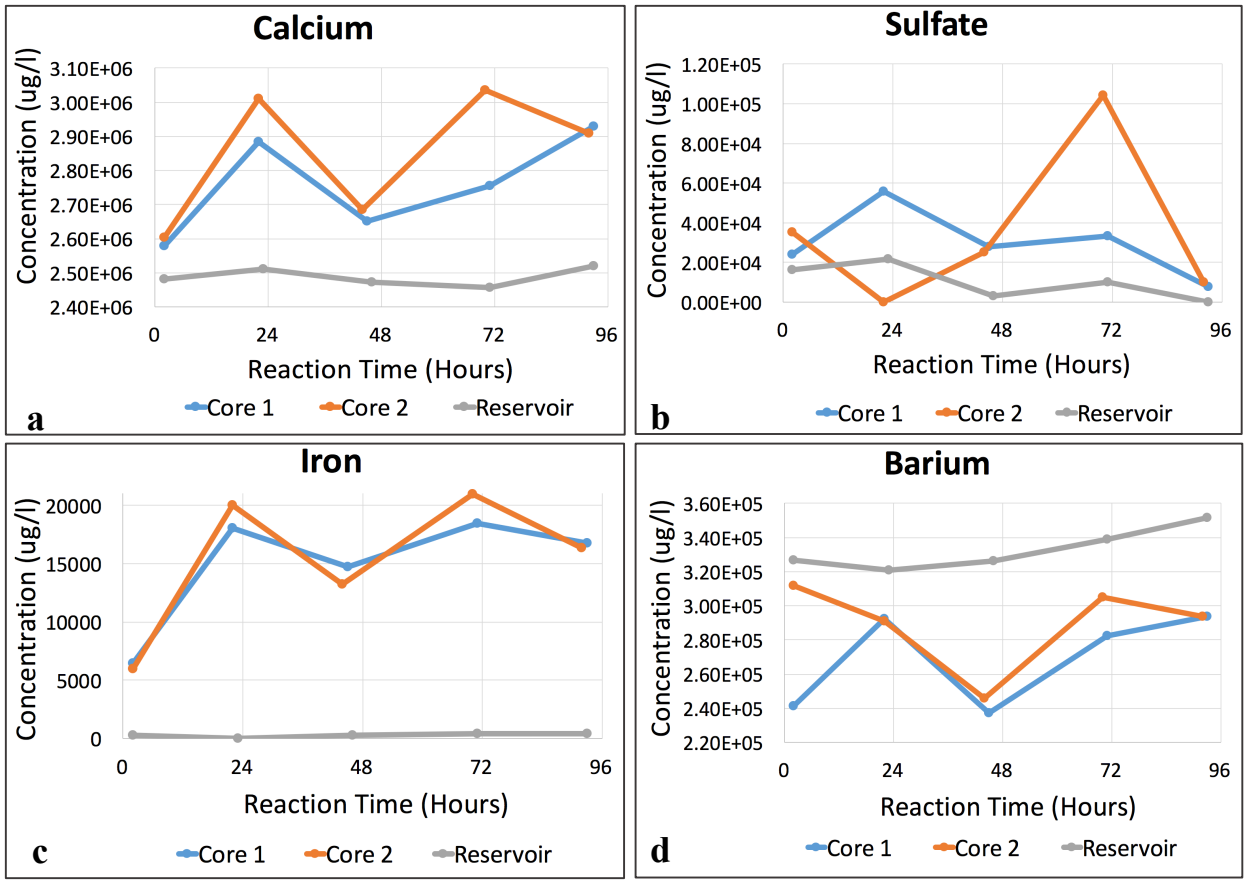

Figure 19: Test 5 calcium (a), sulfate (b), iron (c), and barium (d) concentrations over time from Cores 1 (blue) and 2 (orange) and from the reservoir (grey). Calcium and iron concentrations in the effluent remained higher than the reservoir concentrations. Barium concentration in the effluent for both cores was lower than the reservoir.

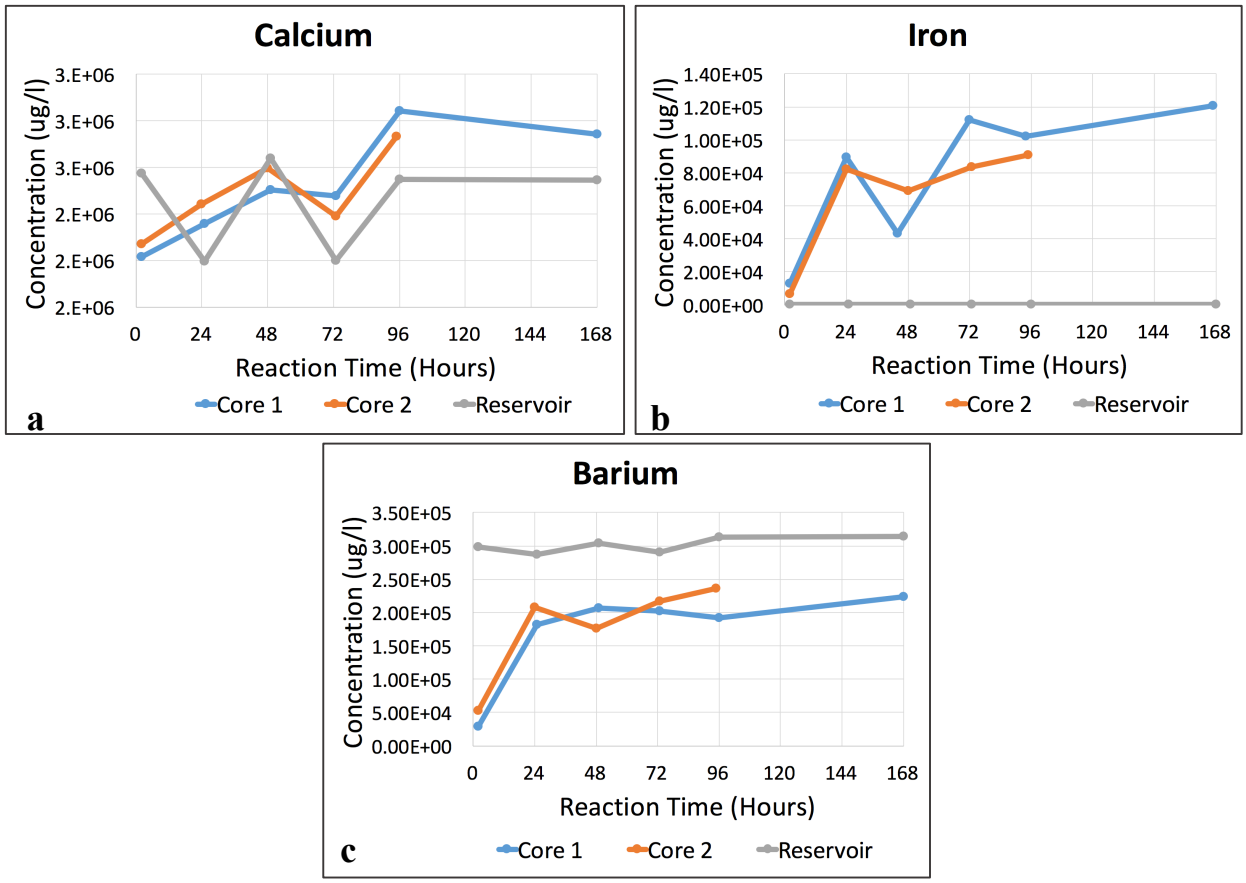

Figure 20: Test 6 calcium (a), iron (b), and barium (c) concentrations over time from Cores 1 (blue) and 2 (orange) and from the reservoir (grey). The reservoir concentration decreases on the small sample days, possibly indicating an error in the calcium concentrations measured from the smaller samples. Calcium in the fluid samples from both cores increased. Iron concentration in the reservoir remained very low while both cores increased in concentration. Barium concentration in the reservoir remained relatively stable and higher than concentrations measured in the effluent. Barium did increase in both cores.

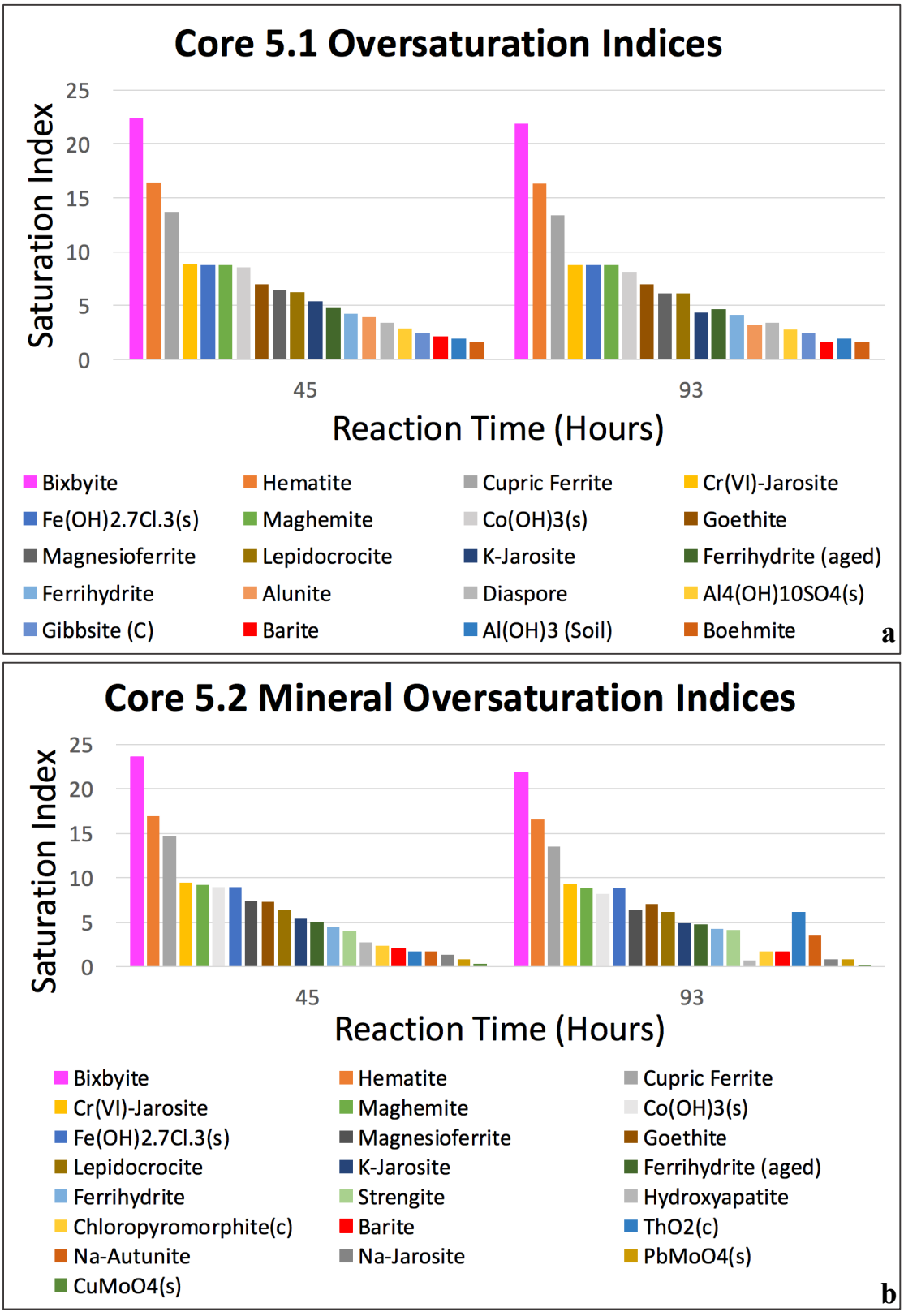

Figure 21: Calculated saturation indices for oversaturated minerals for fluids reacted with cores 5.1 (a) and 5.2 (b). Hematite and other iron rich minerals remained oversaturated. Barite was also slightly oversaturated.

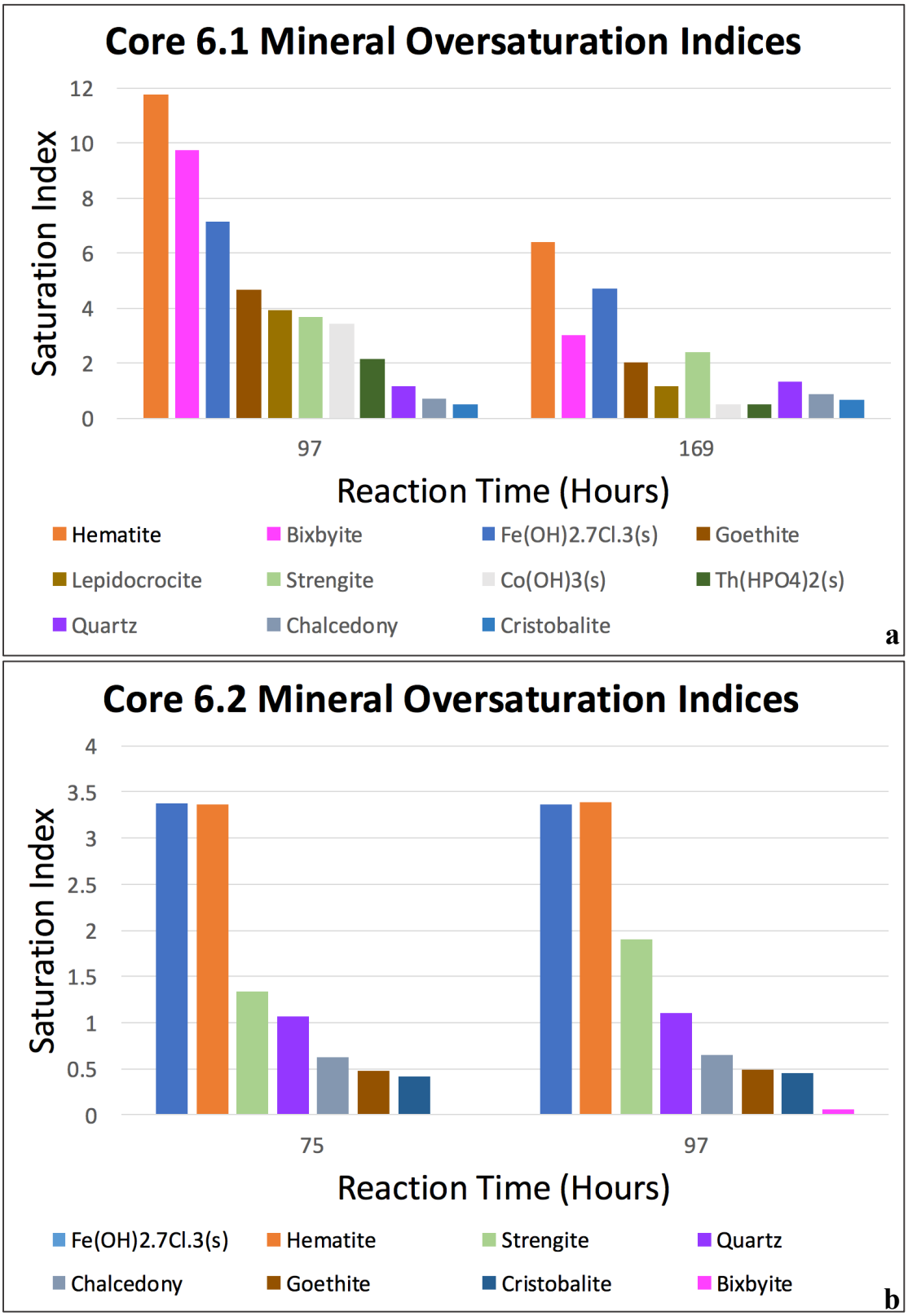

Figure 22: Calculated saturation indices for oversaturated minerals for fluids reacted with cores 6.1 (a) and 6.2 (b). Hematite and other iron rich minerals remained oversaturated. Barite was not oversaturated.

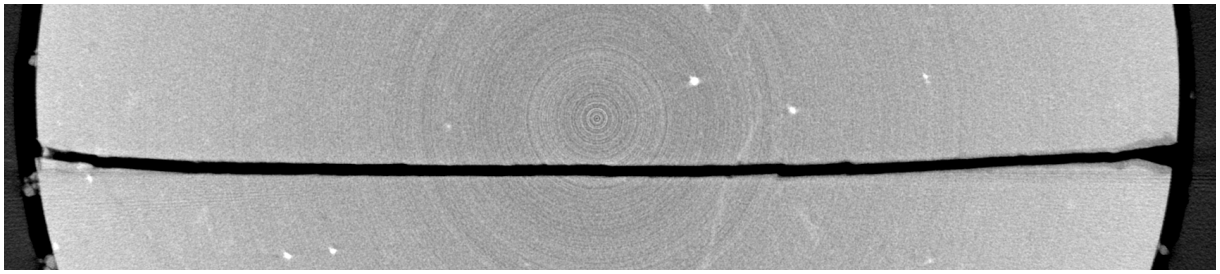

Figure 23: From the bottom of core 2 in test 5, slice number 840 (around 19.57 mm) shows an example of the fracture becoming straight and smooth with very little reaction along the fracture surface.

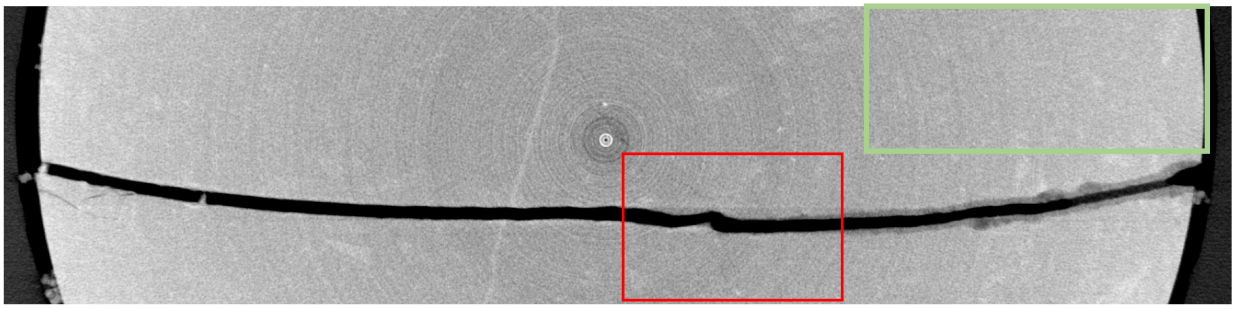

Figure 24: From the bottom of core 2 in test 5, slice number 1346 (around 31.36 mm) shows an example of the fracture becoming rougher, boxed in red. To the right of the bend in the fracture, there is a dark reaction rim around the fracture. There appears to be more calcite in this section, boxed in green.

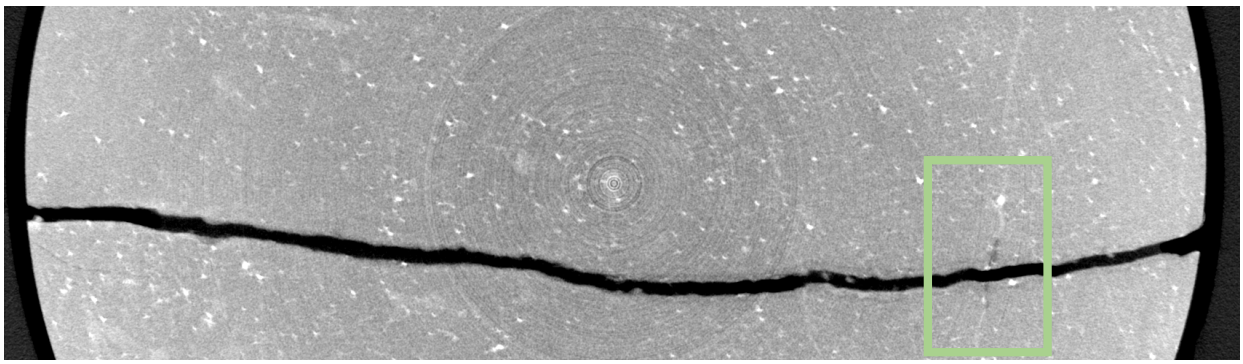

Figure 25: From the bottom of core 2 in test 5, slice number 235 (around 5.48 mm) shows the low reaction in this section except along a calcite vein on the right side, boxed in green. The bright white specks are highly attenuating pyrite nodules.

Table 1: Hydraulic fracturing fluid composition for well MIP 3H from the MSEEL project. Data was reported on FracFocus.org and accessed on October 6, 2017. Additional information on the purpose of additives was found from Table S2 in Vankeuren et al., 2017 (in yellow) and from Stringfellow et al., 2014 (in green).

Trade Name	Supplier	Purpose	Ingredients	Maximum Ingredient Concentration in Additive (% by mass)	Maximum Ingredient Concentration in HF Fluid (% by mass)
Proppant Transport	Schlumberger	Corrosion Inhibitor, Scale Inhibitor, Biocide, AntiFoam Agent, Acid, Breaker, Gelling Agent, Friction Reducer, Iron Control Agent, Fluid Loss Additive			
		Base Fluid	Water (including Mix Water Supplied by Client)		87.63568
		Proppant	Quartz, Crystalline silica	99.06784	12.21724
		Perforation Cleaner	Hydrochloric acid	0.66726	0.08228
		Breaker	Ammonium sulfate	0.06845	0.00844
		Increase fluid viscosity	Guar gum	0.05865	0.00724
		Friction reducer, scale inhibitor	Acrylamide, 2-acrylamido-2-methylpropanesulfonic acid, sodium salt polymer	0.05052	0.00623
		Biocide	Glutaraldeyde	0.02831	0.00349
			Ethanlo, 2,2',2"-nitrilotris-,1,1'1"-tris(dihydrogen phosphate), sodium salt	0.00971	0.00120
		Breaker	Diammonium peroxidisulphate	0.00601	0.00074
		Scale inhibitor	Polymer of 2-acrylamido-2-methylpropanesulfonic acid sodium salt and methyl acrylate	0.00541	0.00067
		Friction reducer	Alkyl(c12-16) dimethylbenzyl ammonium chloride	0.00506	0.00062
		Iron control	Sodium erythorbate	0.00436	0.00054
			Trisodium ortho phosphate	0.00427	0.00053
		Corrosion inhibitor	Urea	0.00332	0.00041
			Polypropylene glycol	0.00294	0.00036
		Gel stabilizer, corrosion inhibitor	Methanol	0.00252	0.00031
		Gelling agent	Fatty acids, tall-oil	0.00156	0.00019
		Corrosion inhibitor	Thiourea, polymer with formaldehyde and 1-phenylethanone	0.00129	0.00016
		Scale inhibitor, corrosion inhibitor	Ethylene Glycol	0.00121	0.00015
			Non-crystalline silica (impurity)	0.00084	0.00010

Trade Name	Supplier	Purpose	Ingredients	Maximum Ingredient Concentration in Additive (% by mass)	Maximum Ingredient Concentration in HF Fluid (% by mass)
			Vinylidene chloride/methylacrylate copolymer	0.00080	0.00010
		Breaker	Sodium sulfate	0.00078	0.00010
			Alcohols, C14-15, ethoxylated (7EO)	0.00061	0.00008
		Gel stabilizer	Ethanol	0.00061	0.00007
		Corrosion inhibitor	Propargyl alcohol	0.00041	0.00005
			2-Propenamid (impurity)	0.00017	0.00002
			Hexadec-1-ene	0.00014	0.00002
			1-Octadecene (C18)	0.00007	0.00001
			Dimethyl siloxanes and silicones	0.00005	0.00001
			Tetrasodium ethylenediaminetetraacetate	0.00009	0.00001
			Dodecamethylcyclohexasiloxane		
			Siloxanes and silicones, dimethyl, reaction products with silica	0.00001	
			Octamethylcyclotetrasiloxane		
			Poly(tetrafluoroethylene)	0.00001	
			Formaldehyde	0.00001	
		Breaker	Copper(II) sulfate		
			Decamethyl cyclopentasiloxane		
			Magnesium silicate hydrate (talc)	0.00002	
FR Pro 150	ECM	Friction Reduction			
			Water	50.00000	0.01575
		Friction reducer	Polyacrylamide-co-acrylic acid	32.00000	0.01008
		Friction reducer	Sodium Chloride	15.00000	0.00472
		Friction reducer	Alcohol Ethoxylate Surfactants	5.00000	0.00157
		Gelling agent, friction reducer	Petroleum Distillate	25.00000	

Table 2: Chemical list of the synthetic fracturing fluid mixed together for tests 5 and 6. A similar composition of hydraulic fracturing fluids was used in previous test at NETL. The additives used were based on the MSEEL hydraulic fracturing fluid list and common additives listed on FracFocus.org.

Additive	Chemical Formula	Amount added in grams per liter of fluid	Amount added in ml per liter of fluid	Why the additive was used
Spring Water		994.54		Cheaper and easier to source water by pumping from a nearby water source
Solid Chemicals				
Citric acid	$C_6H_8O_7$	0.03365	0.0669	Iron control
Boric acid	HBO_3	0.02005	0.0504	Cross linker
Potassium carbonate	K_2CO_3-$10H_2O$	0.23838	0.47676	pH adjuster
Barium chloride dehydrate	$BaCl_2$-$2H_2O$	0.463967	0.92799	
Potassium chloride	KCl	0.216199	0.43240	Clay stabilizer
Strontium chloride sesquihydrate	$SrCl_2$-$6H_2O$	1.35975	2.7195	
Ammonium chloride	NH_4Cl	0.160474	0.32095	Surfactant, cross linker, or biocide
Sodium bromide	NaBr	0.180064	0.36012	
Calcium chloride dehydrate	$CaCl_2$-$2H_2O$	7.424235	14.84847	Breaker
Magnesium chloride sesquihydrate	$MgCl_2$-$6H_2O$	1.870385	3.74077	Breaker
Sodium chloride	NaCl	16.69716	33.39432	Clay stabilizer or breaker
Sodium sulfate	Na_2SO_4	0.000293	0.000586	
Sodium bicarbonate	$NaHCO_3$	0.148058	0.29612	
Liquid Chemicals				
Ethylene glycol	$C_2H_6O_2$	0.089	0.0446	Cross linker
WFR-61LA		0.9888	0.4944	Weatherford proprietary friction reducer
WAI-251LC		0.0254	0.0127	Weatherford proprietary corrosion inhibitor
WGA-15L		2.9664	1.4832	Weatherford proprietary gelling agent
EC6110a		0.3802	0.1901	Nalco biocide (glutaraldehyde)
Hydrochloric acid (37%)		5.0756	2.5378	Perforation cleaner

Table 3: Approximate scale weight for test 5 IC samples. No acid was added to the samples. Small samples collected on test days 1, 2, and 4 were diluted with DI water. The dilution factor was calculated by dividing the total weight by the sample weight.
* The Approx Scale Weight was not recorded on this day

Sample Name	Location	Date	Time	Approx Scale Weight [g]	Dilution Weight [g]	Acid Added [mL]	Total Weight [g]	Dilution Factor
PARA1 42912	A	6/26/17	1700	5 *	----	----	5	1
PARA1 42912	D	6/27/17	1640	5 *	----	----	5	1
PARA2 42912	D	6/28/17	1620	5 *	----	----	5	1
PARA2 42912	B	6/26/17	1730	1 *	4.0202	----	5.0202	5.0202
PARA1 42912	B	6/26/17	1720	1 *	4.0283	----	5.0283	5.0283
PARA1 42913	B	6/27/17	1310	1.0214	4.0194	----	5.0408	4.935186998
PARA2 42913	B	6/27/17	1330	1.0479	3.9924	----	5.0403	4.809905525
PARA1 42913	A	6/27/17	1345	1.0238	4.006	----	5.0298	4.912873608
PARA1 42914	B	6/28/17	1140	5.0087	----	----	5.0087	1
PARA2 42914	B	6/28/17	1150	5.0216	----	----	5.0216	1
PARA1 42914	A	6/28/17	1220	5.024	----	----	5.024	1
PARA1 42915	A	6/29/17	1310	5.0225	----	----	5.0225	1
PARA1 42915	B	6/29/17	1350	1.0024	4.0153	----	5.0177	5.005686353
PARA2 42915	B	6/29/17	1410	1.0035	3.981	----	4.9845	4.967115097
PARA1 42916	A	6/30/17	1115	5.0374	----	----	5.0374	1
PARA1 42916	B	6/30/17	1135	5.4358	----	----	5.4358	1
PARA2 42916	B	6/30/17	1145	5.0041	----	----	5.0041	1
PARA1 42916	D	6/30/17	1210	4.9895	----	----	4.9895	1
PARA2 42916	D	6/30/17	1220	5.0283	----	----	5.0283	1

Table 4: Approximate scale weight for test 5 ICP samples. Nitric acid was added to the samples. Small samples collected on test days 1, 2, and 4 were diluted with DI water. The dilution factor was calculated by dividing the total weight by the sample weight.
* The Approx Scale Weight was not recorded on this day

Sample Name	Location	Date	Time	Approx Scale Weight [g]	Dilution Weight [g]	Acid Added [mL]	Total Weight [g]	Dilution Factor
PARA1 42912	B	6/26/17	1720	1 *	8.9393	0.05	9.9893	9.9893
PARA1 42912	A	6/26/17	1700	10 *	----	0.1	10.1	1.01
PARA1 42912	D	6/26/17	1640	10 *	----	0.1	10.1	1.01
PARA2 42912	B	6/26/17	1730	1 *	8.9589	0.05	10.0089	10.0089
PARA2 42912	D	6/26/17	1620	10 *	----	0.1	10.1	1.01
PARA1 42913	B	6/27/17	1310	1.0095	8.9577	0.05	10.0172	9.922932145
PARA1 42913	A	6/27/17	1345	1.0382	8.9601	0.05	10.0483	9.678578309
PARA2 42913	B	6/27/17	1330	1.0032	8.941	0.05	9.9942	9.962320574
PARA1 42914	B	6/28/17	1140	9.9739	----	0.1	10.0739	1.010026168
PARA1 42914	A	6/28/17	1220	10.0056	----	0.1	10.1056	1.009994403
PARA2 42914	B	6/28/17	1150	9.9992	----	0.1	10.0992	1.0100008
PARA1 42915	B	6/29/17	1350	1.005	8.9455	0.05	10.0005	9.950746269
PARA1 42915	A	6/29/17	1310	9.9948	----	0.1	10.0948	1.010005203
PARA2 42915	B	6/29/17	1410	0.9913	8.929	0.05	9.9703	10.05780289
PARA1 42916	D	6/30/17	1210	10.0131	----	0.1	10.1131	1.009986917
PARA1 42916	B	6/30/17	1135	10.0231	----	0.1	10.1231	1.009976953
PARA1 42916	A	6/30/17	1115	10.0289	----	0.1	10.1289	1.009971183
PARA2 42916	B	6/30/17	1145	9.9831	----	0.1	10.0831	1.010016929
PARA2 42916	D	6/30/17	1220	10.0492	----	0.1	10.1492	1.009951041

Table 5: Approximate scale weight for test 5 Sr Isotope samples. Nitric acid was added to the samples. Small samples collected on test days 1, 2, and 4 were diluted with DI water. The dilution factor was calculated by dividing the total weight by the sample weight.
* The Approx Scale Weight was not recorded on this day

Sample Name	Location	Date	Time	Approx Scale Weight [g]	Dilution Weight [g]	Acid Added [mL]	Total Weight [g]	Dilution Factor
PARA1 42912	A	6/26/17	1700	15 *	----	0.2	15.2	1.013333333
PARA1 42912	D	6/27/17	1640	15 *	----	0.2	15.2	1.013333333
PARA2 42912	D	6/26/17	1620	15 *	----	0.2	15.2	1.013333333
PARA2 42912	B	6/26/17	1730	1 *	8.9282	0.05	9.9782	9.9782
PARA1 42912	B	6/26/17	1720	1 *	8.9551	0.05	10.0051	10.0051
PARA1 42913	B	6/27/17	1310	1.0132	8.9443	0.05	10.0075	9.87712199
PARA2 42913	B	6/27/17	1330	1.0618	8.9614	0.05	10.0732	9.486909022
PARA1 42913	A	6/27/17	1345	0.9984	8.9515	0.05	9.9999	10.01592548
PARA1 42914	B	6/28/17	1140	15.0018	----	0.2	15.2018	1.013331734
PARA2 42914	B	6/28/17	1150	15.012	----	0.2	15.212	1.013322675
PARA1 42914	A	6/28/17	1220	14.969	----	0.2	15.169	1.013360946
PARA1 42915	A	6/29/17	1310	15.0338	----	0.2	15.2338	1.013303356
PARA1 42915	B	6/29/17	1350	1.5089	8.938	0.005	10.4519	6.926834118
PARA2 42915	B	6/29/17	1410	1.0308	8.962	0.005	9.9978	9.699068685
PARA1 42916	A	6/30/17	1115	14.9921	----	0.2	15.1921	1.013340359
PARA1 42916	B	6/30/17	1135	15.024	----	0.2	15.224	1.013312034
PARA2 42916	B	6/30/17	1145	15.0247	----	0.2	15.2247	1.013311414
PARA1 42916	D	6/30/17	1210	15.0039	----	0.2	15.2039	1.013329868
PARA2 42916	D	6/30/17	1220	15.0341	----	0.2	15.2341	1.013303091

Table 6: Temperature and pH measurements for test 5. The pH reader was calibrated on June 27, 2017 using two calibration points (7.0 and 4.0).

Sample Name	Location	Date	Time	pH	Temp [C]
42913 A	A	6/27/17	1418	1.35	21.5
42914 B	B-1	6/28/17	1120	5.62	23.5
42914 B	B-2	6/28/17	1150	5.82	24.2
42914 A	A	6/28/17	1310	1.36	23.6
42915 A	A	6/29/17	1330	1.27	24
42915 B	B-1	6/29/17	1410	5.55	22.5
42916 A	A	6/30/17	1110	1.27	24.4
42916 B	B1	6/30/17	1140	5.55	22.3
42916 B	B2	6/30/17	1150	5.51	23.6
42916 D	D1	6/30/17	1230	6.97	24.5
42917 D	D2	6/30/17	1230	7.02	24.5

Table 7: Approximate scale weight for test 6 IC samples. No acid was added to the samples. Small samples collected on test days 1, 2, and 4 were diluted with DI water. The dilution factor was calculated by dividing the total weight by the sample weight.
* The pump for core 1 continued to fail even with several hours of problem solving. Eventually the core had to be removed and the test restarted for core 1.

Sample Name	Location	Date	Time	Approx Scale Weight [g]	Dilution Weight [g]	Acid Added [mL]	Total Weight [g]	Dilution Factor
PARA1 42926	B	7/10/17	1535	0.9818	3.997	----	4.9788	5.071093909
PARA1 42926	A	7/10/17	1545	4.9988	----	----	4.9988	1
PARA2 42926	B	7/10/17	1600	1.0037	3.982	----	4.9857	4.967320913
PARA2 42926	D	7/10/17	1620	5.0167	----	----	5.0167	1
PARA1 42926	D	7/10/17	1630	4.9947	----	----	4.9947	1
PARA1 42927	B	7/11/17	1320	1.0153	3.987	----	5.0023	4.926918152
PARA2 42927	B	7/11/17	1340	1.0124	3.9713	----	4.9837	4.922659028
PARA1 42927	A	7/11/17	1410	1.0015	3.9764	----	4.9779	4.970444333
PARA1 42928	B *	7/12/17	950	4.9907	----	----	4.9907	1
PARA2 42928	B	7/12/17	1325	5.0062	----	----	5.0062	1
PARA1 42928	A	7/12/17	1400	4.9747	----	----	4.9747	1
PARA1 42929	A	7/13/17	1415	1.0164	4.0154	----	5.0318	4.950609996
PARA1 42929	B	7/13/17	1435	1.0011	4.0088	----	5.0099	5.004395165
PARA2 42929	B	7/13/17	1500	1.0173	3.98	----	4.9973	4.912316917
PARA1 42930	B	7/14/17	1220	5.0073	----	----	5.0073	1
PARA2 42930	B	7/14/17	1250	4.9706	----	----	4.9706	1
PARA1 42930	A	7/14/17	1320	4.9998	----	----	4.9998	1
PARA2 42930	D	7/14/17	1420	4.9962	----	----	4.9962	1
PARA1 42933	B	7/17/17	1320	4.9902	----	----	4.9902	1
PARA1 42933	A	7/17/17	1400	5.0219	----	----	5.0219	1
PARA1 42933	D	7/17/17	1500	4.972	----	----	4.972	1

Table 8: Approximate scale weight for test 6 ICP samples. Nitric acid was added to the samples. Small samples collected on test days 1, 2, and 4 were diluted with DI water. The dilution factor was calculated by dividing the total weight by the sample weight.
* The pump for core 1 continued to fail even with several hours of problem solving. Eventually the core had to be removed and the test restarted for core 1.

Sample Name	Location	Date	Time	Approx Scale Weight [g]	Dilution Weight [g]	Acid Added [mL]	Total Weight [g]	Dilution Factor
PARA1 42926	B	7/10/17	1535	1.024	8.9523	0.05	10.0263	9.791308594
PARA1 42926	A	7/10/17	1545	10.1379	----	0.1	10.2379	1.009863976
PARA2 42926	B	7/10/17	1600	0.999	8.9551	0.05	10.0041	10.01411411
PARA2 42926	D	7/10/17	1620	9.994	----	0.1	10.094	1.010006004
PARA1 42926	D	7/10/17	1630	9.9936	----	0.1	10.0936	1.010006404
PARA1 42927	B *	7/11/17	1320	0.9959	8.9265	0.05	9.9724	10.01345517
PARA2 42927	B	7/11/17	1340	0.9901	8.9516	0.05	9.9917	10.09160691
PARA1 42927	A	7/11/17	1410	0.9889	8.943	0.05	9.9819	10.09394276
PARA1 42928	B	7/12/17	950	9.96	----	0.1	10.06	1.010040161
PARA2 42928	B	7/12/17	1325	9.9939	----	0.1	10.0939	1.010006104
PARA1 42928	A	7/12/17	1400	9.9892	----	0.1	10.0892	1.010010812
PARA1 42929	A	7/13/17	1415	0.9913	8.949	0.05	9.9903	10.07797841
PARA1 42929	B	7/13/17	1435	1.0069	8.9364	0.05	9.9933	9.924818751
PARA2 42929	B	7/13/17	1500	1.0118	8.9255	0.05	9.9873	9.870824274
PARA1 42930	B	7/14/17	1220	10.0021	----	0.1	10.1021	1.0099979
PARA2 42930	B	7/14/17	1250	9.9756	----	0.1	10.0756	1.01002446
PARA1 42930	A	7/14/17	1320	9.9859	----	0.1	10.0859	1.01001412
PARA2 42930	D	7/14/17	1420	10.0016	----	0.1	10.1016	1.0099984
PARA1 42933	B	7/17/17	1320	9.975	----	0.1	10.075	1.010025063
PARA1 42933	A	7/17/17	1400	9.967	----	0.1	10.067	1.010033109
PARA1 42933	D	7/17/17	1500	9.984	----	0.1	10.084	1.010016026

Table 9: Approximate scale weight for test 6 Sr Isotope samples. Nitric acid was added to the samples. Small samples collected on test days 1, 2, and 4 were diluted with DI water. The dilution factor was calculated by dividing the total weight by the sample weight.
* The pump for core 1 continued to fail even with several hours of problem solving. Eventually the core had to be removed and the test restarted for core 1.

Sample Name	Location	Date	Time	Approx Scale Weight [g]	Dilution Weight [g]	Acid Added [mL]	Total Weight [g]	Dilution Factor
PARA1 42926	B	7/10/17	1535	0.9984	8.932	0.05	9.9804	9.996394231
PARA1 42926	A	7/10/17	1545	15.0043	----	0.2	15.2043	1.013329512
PARA2 42926	B	7/10/17	1600	1.0129	8.9313	0.05	9.9942	9.866916774
PARA2 42926	D	7/10/17	1620	15.0092	----	0.2	15.2092	1.013325161
PARA1 42926	D	7/10/17	1630	14.9916	----	0.2	15.1916	1.013340804
PARA1 42927	B *	7/11/17	1320	0.993	8.94	0.05	9.983	10.05337362
PARA2 42927	B	7/11/17	1340	1.0004	8.9419	0.05	9.9923	9.988304678
PARA1 42927	A	7/11/17	1410	0.9986	8.9455	0.05	9.9941	10.00811136
PARA1 42928	B	7/12/17	950	14.9814	----	0.2	15.1814	1.013349887
PARA2 42928	B	7/12/17	1325	15.0032	----	0.2	15.2032	1.013330489
PARA1 42928	A	7/12/17	1400	15.0156	----	0.2	15.2156	1.013319481
PARA1 42929	A	7/13/17	1415	0.9955	8.929	0.05	9.9745	10.01958815
PARA1 42929	B	7/13/17	1435	0.9878	8.9423	0.05	9.9801	10.103361
PARA2 42929	B	7/13/17	1500	1.017	8.9342	0.05	10.0012	9.834021632
PARA1 42930	B	7/14/17	1220	14.9819	----	0.2	15.1819	1.013349442
PARA2 42930	B	7/14/17	1250	14.9765	----	0.2	15.1765	1.013354255
PARA1 42930	A	7/14/17	1320	14.9958	----	0.2	15.1958	1.013337068
PARA2 42930	D	7/14/17	1420	14.9733	----	0.2	15.1733	1.013357109
PARA1 42933	B	7/17/17	1320	14.9745	----	0.2	15.1745	1.013356039
PARA1 42933	A	7/17/17	1400	14.9869	----	0.2	15.1869	1.013344988
PARA1 42933	D	7/17/17	1500	14.975	----	0.2	15.175	1.013355593

Table 10: Temperature and pH measurements for test 6. The pH reader was calibrated on June 27, 2017 using two calibration points (7.0 and 4.0).

Sample Name	Location	Date	Time	pH	Temp [C]
42926 A	A	7/10/17	1610	1.12	26.2
42929 A	A	7/13/17	1420	0.98	23.5
42929 B2	B2	7/13/17	1520	1.87	23
42930 B1	B1	7/14/17	1310	3.44	22.1
42930 B2	B2	7/14/17	1310	1.87	23.3
42930 A	A	7/14/17	1420	1.07	23.9
42930 D2	D2	7/14/17	1440	6.96	23.5
42933 B1	B1	7/17/17	1345	2.33	24
42933 A	A	7/17/17	1430	0.97	22.5
42933 D1	D1	7/17/17	1505	8.22	26.1

Appendix A

Image Processing Appendix

Initial Image Processing of CT Images

The original images from the CT scan lack contrast and the images extend beyond usable parts of the cores (Figure A1). The contrast was corrected by selecting Adjust from the Image drop down menu. By clicking Auto under Brightness/Contrast once, the image contrast was corrected automatically (Figure A2). The ends of the cores needed to be cropped due to feedback from the metal endbells. Scrolling through the top and the bottom halves of the cores, I visually determined which slices needed to be cropped. To speed up later image processing steps, I cropped the image to just the fracture area to reduce the file size. Cropping the ends of the cores, while necessary, assumes any rock core alterations will occur beyond the cutoff points I selected.

Image Segmentation

To identify and characterize the fracture, proppant, and reaction rim, the processed images were then segmented using Ilastik, a free image software. The pixel classification workflow was used in Ilastik. The same feature selected was used on every CT image from tests 5 and 6 (Figure A3). Following the workflow, the next step was to train the program by creating labels for the matrix, proppant, fracture, and water. For each label, I identified corresponding pixels (Figure A4). Using the pixels I manually identified, Ilastik classified the rest of the core. With some corrections, eventually Ilastik provided a reasonable classification of the core based off of the four labels (Figure A5). Segmentation based on the pixel classification was then exported from Ilastik. Using Ilastik to classify pixels assumes I corrected the program classification enough to have a high enough prediction. It was not possible to look through each slice for errors.

The segmented images were then opened in ImageJ for quantitative analysis. Although Ilastik provided a good estimate for the four categories, there were still some errors and noise that needed to be cleaned up. I created an ImageJ workflow to remain consistent while processing the images for each core (Table 1). To calculate the distribution of proppant before and after the test, outliers classified as proppant needed to be removed and holes in the proppant needed to be filled (Figures A6-A8). Cleaning up the images assumes the proppant pieces were all large enough not to be removed and the edges of the proppant pieces were minimally altered.

Fractional Area

To quantify the amount of the fracture surface that reacted, the segmented sections needed to be edited and overlapped. In ImageJ the outline tool was used on the fracture and the reaction rim segmentation layers. The outline was then dilated on each layer. In each layer the outline was given a value of 1 while the rest of the image had a value of 0. Adding the two layers together created a new layer with pixels represented as a 2, 1, or 0. Selecting just pixels with a value of 2 gave me the area of the fracture surface that reacted. Measuring the proppant volume

throughout the core assumes the proppant did not move too much when the sample was moved from the experimental apparatus to the CT scanner.

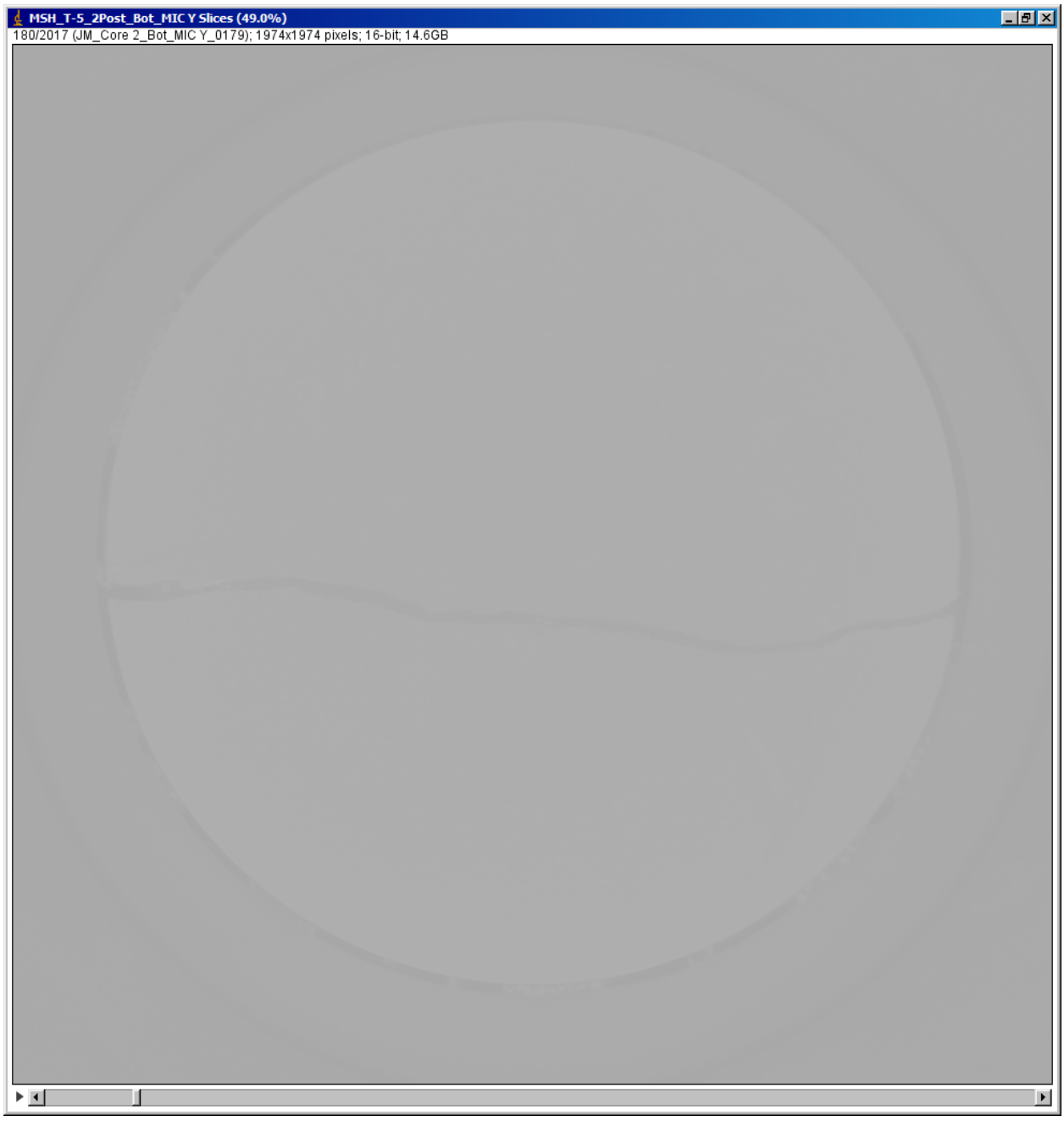

Figure A1: An example CT images in ImageJ before editing and cropping. The core is somewhat visible with the horizontal fracture. From the center of the image there is the core, then a small amount of air, the rubber casing, and then air.

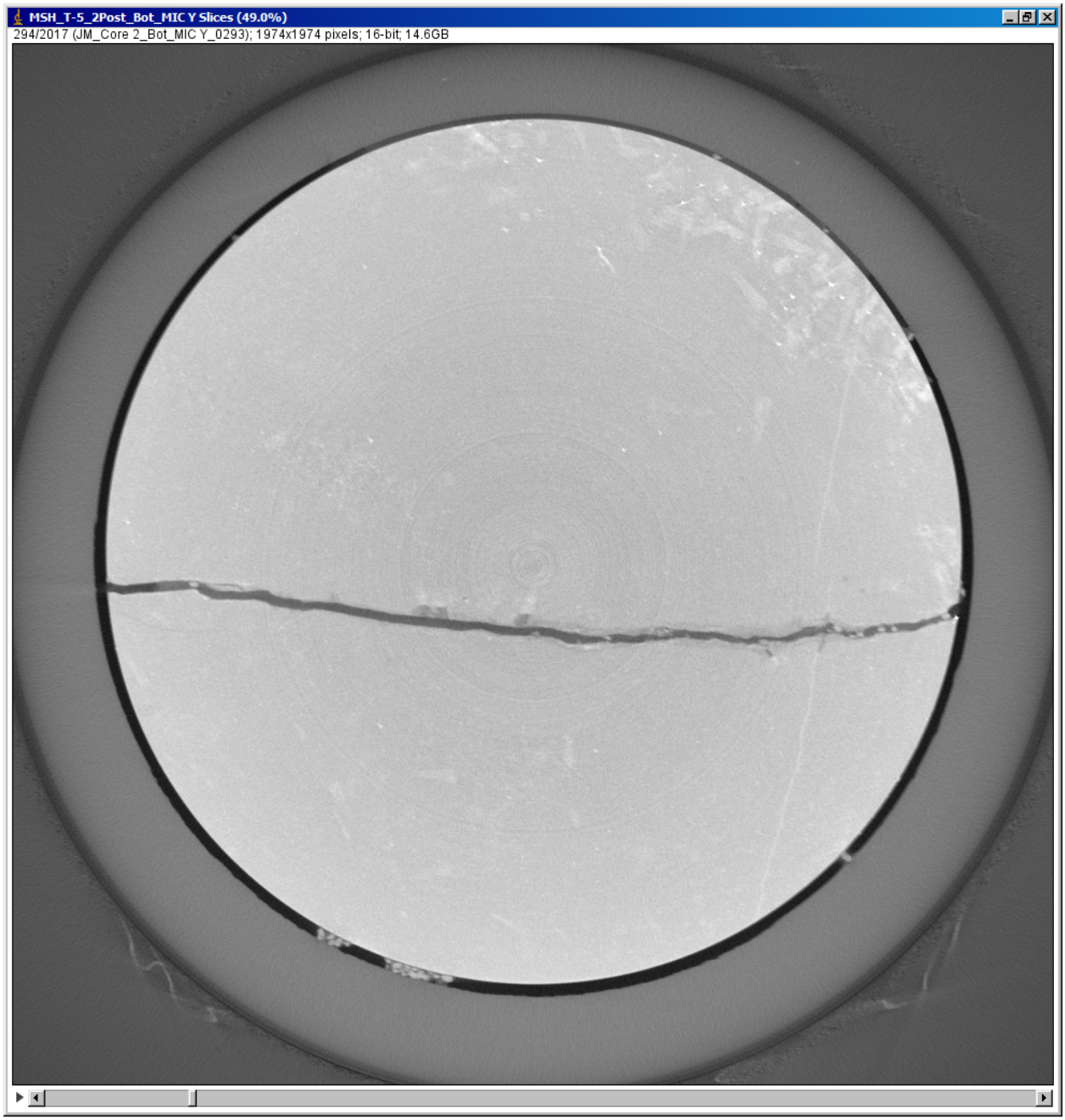

Figure A2: The same image from Figure 6 but with the brightness and contrast corrected by selecting Adjust from the Image drop down menu. Clicking "Auto" under Brightness/Contrast once was enough for me to clearly identify the fracture for cropping.

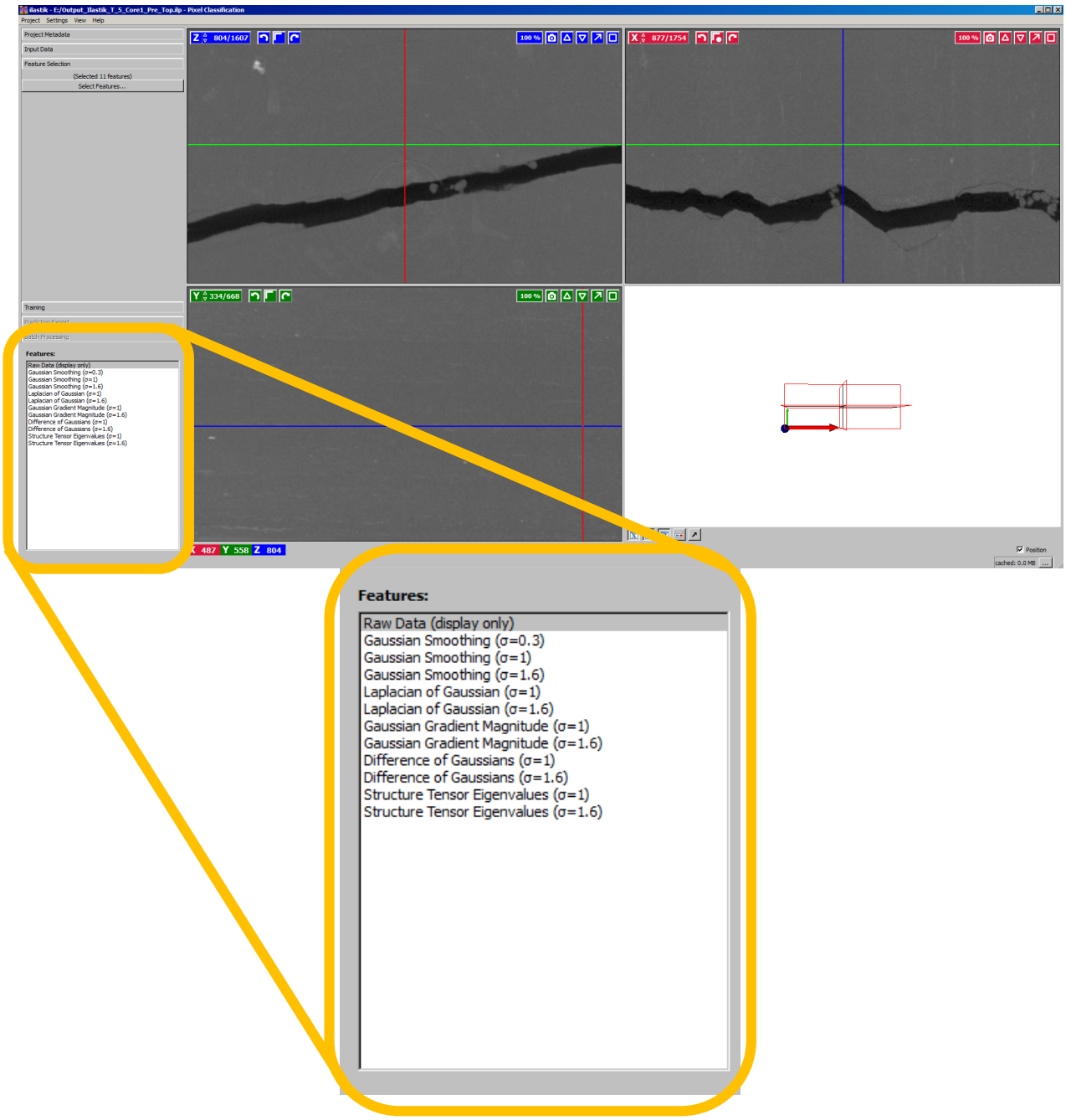

Figure A3: Ilastik feature selection window for CT images. The features were selected for improving visual identification of pixels on a greyscale.

Figure A4: From test 5, a screenshot from the training tab in the pixel classification workflow in Ilastik. Labels were created for the matrix (red), proppant (green), fracture (yellow), and water(blue). For each label, pixels were manually identified.

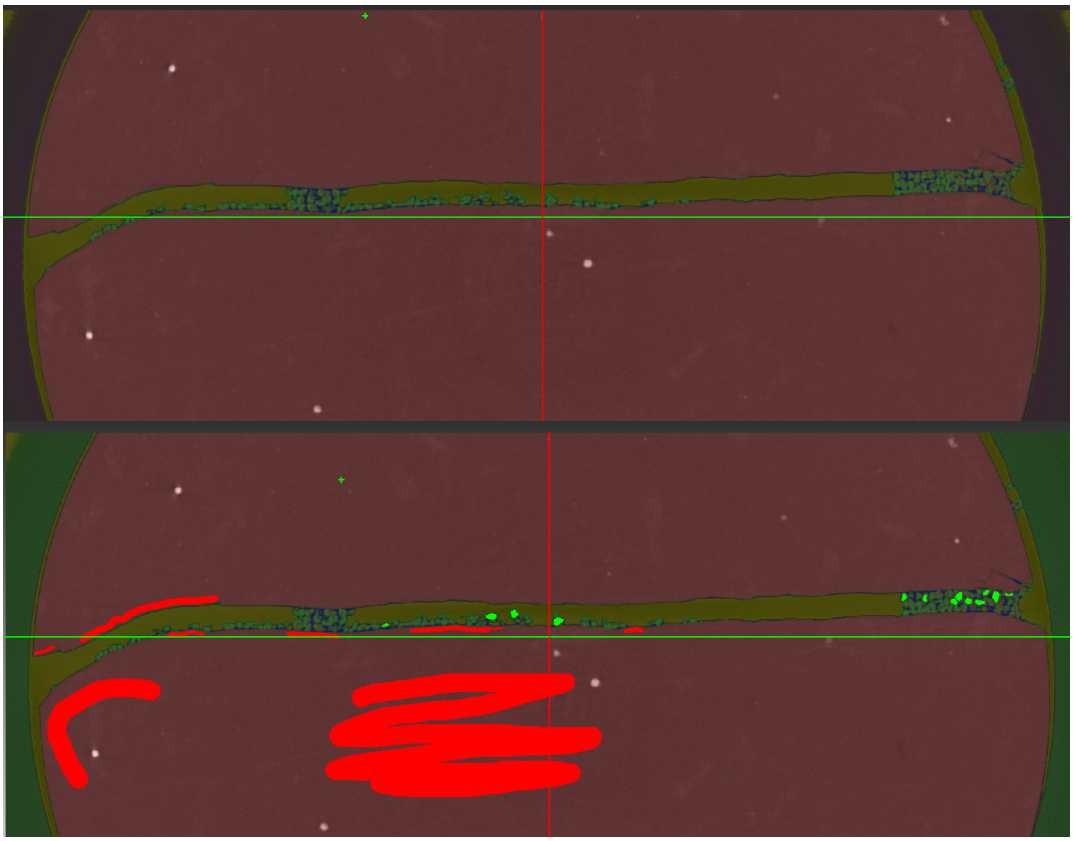

Figure A5: Ilastik images from test 5 of the same slice, demonstrating some of the manual corrections needed after running the program to classify pixels.

Figure A6: The segmented image from Ilastik in ImageJ. Following the work flow I created (Table 1), an ROI (region of interest; thin yellow line) was created to crop out the are outside of the rock core. In the center, in white, are the proppant grains in the fracture.

Figure A7: The same slice as figure 11 but with the area outside the rock core cropped.

Figure A8: Continuing to follow the workflow from Table 1, the image shows the proppant after removing the outliers.

Table A1: ImageJ workflow I used to isolate the proppant from the segmented images. I compared two variations and found that by filling in the proppant pieces, there was a larger loss in definition of the grains.

Output_ImageJ_T_5_Core1_Pre_Top_Analysis	
Change Applied	**Notes**
Image > Adjust > Brightness/Contrast Hit Auto once	This makes it possible to see the three values instead of just a black image
Image > Adjust > Threshold Select just the proppant (slide bars to 2) Hit Apply and make sure only "Black Background (of binary masks) is selected	This selects the value you want to look at – In this case we are looking at the proppant
Create a circular ROI that will crop out the white area around the core Then go to Image > crop Edit > Clear Outside	Need to crop out the area beyond the core
Right click on the image > Duplicate Select Duplicate Stack	Duplicates the entire image stack just in case you make a change that you don't like
Process > Noise > Remove Outliers Radius: 2.0 pixels Which outliers: Bright	This gets rid of the bright spots that are not proppant
Right click on the image > Duplicate Select Duplicate Stack (2^{nd} duplicate)	Duplicates the entire image stack just in case you make a change that you don't like
Edit > Invert	This inverts the black and white colors
Process > Binary > Fill Holes	Fills in holes
Right click on the image > Duplicate Select Duplicate Stack (3^{rd} duplicate)	Duplicates the entire image stack just in case you make a change that you don't like and to compare tools
Process > Noise > Remove Outliers on 3^{rd} duplicate Radius: 2.0 pixels Which outliers: Dark	This gets rid of the dark spots that are not proppant
Analyze > Set Measurements 3^{rd} duplicate Only select Are and Area Fraction	Tells ImageJ what to measure – We want to know the distribution of the proppant so we just want the area.
Plugins > Stacks > Measure Stack 3^{rd} duplicate	This pulls up the area for every slice
Right click on the image > Duplicate Select Duplicate Stack (4^{th} duplicate)	Duplicates the entire image stack just in case you make a change that you don't like and to compare tools
Edit > Invert the 4^{th} duplicate	This inverts the black and white colors
Process > Noise > Remove Outliers on 4^{th} duplicate Radius: 2.0 pixels Which outliers: Dark	This gets rid of the dark spots inside of the proppant
Plugins > Stacks > Measure Stack 4^{th} duplicate	This pulls up the area for every slice
Comparing the 3^{rd} and 4^{th} duplicates – the 3^{rd} looks the best	